IMMUNOLOGY

Regulation of autoimmune disease progression by Pik3ip1 through metabolic reprogramming in T cells and therapeutic implications

Wenqiang Xie[1]†, Juan Fang[1]†, Zhongyan Shan[1]†, Junyi Guo[1]†, Yuan Liao[2], Zhaolei Zou[1], Jun Wang[3], Shuqiong Wen[1], Lisa Yang[1], Yanshu Zhang[1], Huanzi Lu[1], Hang Zhao[4], Dong-Ming Kuang[5], Peng Huang[6], Qianming Chen[7], Zhi Wang[1]*

Metabolic alterations could profoundly affect immune functions and influence the progression and outcome of autoimmune diseases. However, the detailed mechanisms and their therapeutic potential remain to be defined. Here, we show that phosphatidylinositide 3-kinase interacting protein 1 (Pik3ip1), a newly identified negative immune regulator, is notably down-regulated in several major autoimmune diseases through a previously unidentified mechanism mediated by interleukin-21/p38 mitogen-activated protein kinase/a disintegrin and metalloprotease-17 (ADAM17) pathway. Down-regulation of Pik3ip1 in T cells causes a major metabolic shift from oxidative phosphorylation toward aerobic glycolysis, leading to their overactivation and aggressive disease progression in experimental autoimmune encephalomyelitis (EAE) mouse model. Suppression of hypoxia-inducible factor 1α (Hif1α) or pharmacologic inhibition of glycolysis could reverse these phenotypes and largely mitigate EAE severity. Our study reveals a previously unrecognized role of Pik3ip1 in metabolic regulation that substantially affects the inflammatory loop in the autoimmune setting and identifies the Pik3ip1/Hif1α/glycolysis axis as a potential therapeutic target for treatment of autoimmune diseases.

INTRODUCTION

Autoimmune diseases involve a group of disorders characterized by a condition where the adaptive immune system reacts against self-antigens, leading to localized or systemized inflammation and tissue destruction. The underlying mechanisms of autoimmunity remain still incompletely elucidated, but it appears that autoimmune diseases initiate or exacerbate due to the loss of immunological tolerance (*1*). T lymphocytes are the central players in regulating adaptive immune responses. The impairment of T cell tolerance, which polarizes T cells into hyperactive and pathogenic inflammatory phenotypes, will lead to both T cell/autoantibody-mediated autoimmune diseases (*2*, *3*). Therefore, it is urgent to develop therapies that aim to enhance T cell tolerance and restrain pathogenic inflammatory T cells to various kinds of T cell–mediated autoimmune diseases in preclinical and clinical trials (*4*, *5*). However, the mechanisms by which T cells turn into inflammatory phenotypes are poorly understood. A deeper understanding of the external or intrinsic factors that drive the polarization of T cells will help identify novel targets in the treatment of autoimmune diseases.

Alterations in metabolic programs of T cells are intricately linked with their activation and inflammatory status (*6*, *7*). Although growing evidence has suggested that aerobic glycolysis endows T cells with strong proinflammatory phenotype both transcriptionally and epigenetically (*8*, *9*), the molecular pathway that switches the oxidative quiescent T cells toward glycolytic proinflammatory T cells remains unclear. Negative immune regulators, such as cytotoxic T-lymphocyte associated protein-4 (CTLA-4), programmed cell death protein-1 (PD-1), and lymphocyte activation gene-3 (LAG-3), are proteins that conduct negative signals of immune activation and thwart inappropriate immune responses. It has been demonstrated that negative immune regulators are required to suppress glycolysis and drive oxidative metabolism in T cells during infection and tumor (*10*–*12*). However, whether they participate in T cell metabolic reprogramming under autoimmune conditions is not thoroughly explored. Up till now, only one drug (abatacept, a CTLA-4–Fc fusion protein) that targets negative immune regulators has been given full approval by the U.S. Food and Drug Administration for treatment of several autoimmune diseases, but the response rate was unsatisfactory (*13*). Thus, it is of great necessity to thoroughly understand the underpinning metabolic regulation by negative immune regulators and find more effective alternatives in autoimmune diseases.

Phosphatidylinositide 3-kinase interacting protein 1 (Pik3ip1) is an upstream inhibitor of phosphatidylinositol 3-kinase (PI3K) signaling with a kringle domain on the cell surface and a cytoplasmic domain that contains a motif homologous to the PI3K regulatory subunit p85 (*14*–*16*). Previous studies have reported that Pik3ip1, which is highly expressed on naïve T cells (Tn) and rapidly reduced its expression upon T cell activation, plays an essential role in regulating T cell–mediated responses (*16*–*18*). We previously defined Pik3ip1 as a novel negative immune regulator in the context of tumor that restrained T cell–mediated antitumor response (*18*). Nevertheless, whether Pik3ip1 is involved in T cell metabolic regulation and its role in the polarization of proinflammatory T cells during autoimmunity is scarcely explored.

In this study, we demonstrate that the down-regulation of Pik3ip1 in T cells is prevalent in patients with autoimmune diseases, e.g.,

[1]Guanghua School of Stomatology, Guangdong Provincial Key Laboratory of Stomatology, Stomatological Hospital, Sun Yat-Sen University, Guangzhou 510055, China. [2]Department of Laboratory Medicine, The Third Affiliated Hospital of Sun Yat-sen University, Guangzhou, China. [3]Department of Pathology, New York University Grossman School of Medicine, New York, NY, USA. [4]State Key Laboratory of Oral Diseases, Chinese Academy of Medical Sciences Research Unit of Oral Carcinogenesis and Management, West China Hospital of Stomatology, Sichuan University, Chengdu, China. [5]Key Laboratory of Gene Engineering of the Ministry of Education, State Key Laboratory of Biocontrol, School of Life Sciences, Sun Yat-sen University, Guangzhou, China. [6]Sun Yat-Sen University Cancer Center, State Key Laboratory of Oncology in South China, Collaborative Innovation Center for Cancer Medicine, Guangzhou, China. [7]School of Stomatology, Zhejiang University School of Medicine, Hangzhou, China.
*Corresponding author. Email: wangzh75@mail.sysu.edu.cn
†These authors contributed equally to this work.

systemic lupus erythematosus (SLE), rheumatoid arthritis (RA), and multiple sclerosis (MS), and the expression level of Pik3ip1 is highly associated with disease severity and treatment response. Mechanistically, the loss of Pik3ip1 expression results in reduced oxidative phosphorylation (OXPHOS) and enhanced glycolysis in T cells, which promotes inflammatory responses and further exacerbates the autoimmune diseases upon initial onset in a hypoxia-inducible factor 1α (Hif1α)–dependent manner. Furthermore, we found that excessive interleukin-21 (IL-21) production in the autoimmune environment contributes to the cleavage of the functional domain of Pik3ip1 through p38 mitogen-activated protein kinase (MAPK)–mediated a disintegrin and metalloprotease-17 (ADAM17) up-regulation. These findings establish Pik3ip1 as a key regulator of T cell metabolic homeostasis and highlight the importance of the Pik3ip1/Hif1α/glycolysis axis in autoimmune diseases.

RESULTS

Down-regulation of Pik3ip1 correlates with the progression of multiple autoimmune diseases

To determine the role of Pik3ip1 in autoimmune diseases, we first sought to examine the expression of Pik3ip1 in patients with autoimmune disease including SLE, RA, or MS. Peripheral blood mononuclear cells (PBMCs) from a total number of 113 patients with autoimmune diseases (57 SLE, 28 RA, and 28 MS) and 10 healthy donors (HDs) were collected for flow cytometric analysis (fig. S1A). Baseline clinical and laboratory data of all patients are depicted in table S1. It has been reported that negative immune regulators including PD-1, CTLA-4, and V-domain immunoglobulin suppressor of T cell activation (VISTA) are likely to up-regulate their expression on T cells in many autoimmune diseases (*19*, *20*). Unexpectedly, we found that the proportion of Pik3ip1$^+$ T cells was significantly reduced in PBMCs from all patient cohorts compared with HDs, irrespective of their disease type (Fig. 1A), suggesting a distinct expression pattern from other classical negative immune regulators during autoimmunity. In support of this, we observed an inverse correlation between the percentage of Pik3ip1$^+$ T cells and the median fluorescence intensity (MFI) of VISTA in T cells (fig. S1B). Furthermore, we analyzed four published bulk RNA sequencing (RNA-seq) datasets for *Pik3ip1* expression to validate our flow cytometric data. Consistently, *Pik3ip1* was found to be markedly decreased in patients with SLE, RA, MS, or Sjögren's syndrome (SS) compared with HDs (fig. S1C). These findings led us to investigate the role of Pik3ip1 in the autoimmune setting.

The reduction in Pik3ip1 expression was more pronounced in patients with later-stage disease. We observed a stepwise reduction in *Pik3ip1* expression as the disease activity of SLE progressed from one to three. In contrast, the recovery of *Pik3ip1* expression was associated with symptom relief in patients with MS. We also assessed the effect of treatment on the expression of *Pik3ip1* in patients with autoimmune diseases. Patients with RA showed up-regulation in *Pik3ip1* to the level similar in that of HDs after anti–tumor necrosis factor (TNF) treatment or even higher after disease-modifying antirheumatic drug (DMARD) administration. In patients with MS with paired PBMC samples, before and after first-line treatment, the treatment also markedly increased the proportion of Pik3ip1$^+$ T cells (Fig. 1B). Furthermore, we investigated the relationship between Pik3ip1 expression and clinical parameters in SLE, RA, and MS. Our results showed that the proportion of Pik3ip1$^+$ T cells was negatively correlated with serum C-reactive protein (CRP) and erythrocyte sedimentation rate (ESR) levels in patients with SLE, RA, or MS. In patients with MS, we also observed an inverse correlation between the proportion of Pik3ip1$^+$ T cells in peripheral blood and expanded disability status scale score, a most common measurement of MS severity. Reduced Pik3ip1$^+$ T cells were shown to be correlated with increased level of serum anti–double-stranded DNA (dsDNA) antibody in patients with SLE (Fig. 1C). In addition, further receiver operating characteristic (ROC) curve analysis demonstrated that down-regulation of Pik3ip1 served as a strong diagnostic biomarker for SLE, RA, and MS, with all the area under the curve (AUC) values of >0.9 (Fig. 1D).

Aberrant activation and function of T cells have been implicated in the development of many autoimmune diseases (fig. S1D) (*20*–*23*). Given the strong relationship between the down-regulation of Pik3ip1 expression and disease progression, we next addressed whether the reduced Pik3ip1 expression was associated with T cell hyperactivity under autoimmune condition. In support of our hypothesis, the percentage of Pik3ip1$^+$ T cells was shown to be proportional to the percentage of Tn, whereas negatively related to the percentages of effector memory T cell (Tem) and terminally differentiated effector memory T cells (Temra) in both CD4$^+$ and CD8$^+$ compartments. Notably, compared to the correlations observed in CD4$^+$ T cells, those in CD8$^+$ T cells displayed smaller dispersion (Fig. 1, E and F). However, there was no significant correlation between the percentage of Pik3ip1$^+$ T cells and the percentage of central memory T cells (Tcm; CD45RA$^-$CCR7$^+$) in either CD4$^+$ or CD8$^+$ lineage (fig. S1E). Furthermore, reduced Pik3ip1 expression on T cells was shown to be associated with increased production of proinflammatory cytokines by T cells, including IL-17, TNF-α, interferon-γ (IFN-γ), and IL-2, although the difference regarding IL-2 was not statistically significant (Fig. 1, E and F, and fig. S1F). In addition, we reanalyzed a published single-cell RNA-seq dataset (*24*) on PBMCs from patients with SS and HDs to further confirm these findings (fig. S1, G and H). We found that *Pik3ip1* was shown to be grouped together with quiescence-associated genes by unsupervised clustering method, indicating that *Pik3ip1* and these genes were closely related and shared similar expression profiles, which were opposite to those of effector genes (fig. S1, H and K). We also noticed that Pik3ip1$^+$ T cells or Tns, which exhibited the highest Pik3ip1 expression among all clusters, markedly reduced cell abundance in the SS group compared with HDs, while the proportion of effector T cells with low Pik3ip1 expression was significantly higher in SS group than HDs (fig. S1, I and J), in accordance with the role of T cell activation in inducing inflammatory infiltration and tissue damage in SS (*25*). Together, we observed a consistent down-regulation of Pik3ip1 expression in multiple autoimmune diseases and the expression of Pik3ip1 highly correlates with disease severity, treatment response, and T cell activation status and proinflammatory profile.

Increased IL-21 expression drives the down-regulation of Pik3ip1 under autoimmune condition

Next, we investigated the potential mechanisms of autoimmunity-induced Pik3ip1 reduction. It is well recognized that autoimmune responses are closely associated with the occurrence of excessive inflammation. We therefore tested whether proinflammatory cytokines were involved in the down-regulation of Pik3ip1 during autoimmunity. We found that, in patients with SLE, RA, or MS, Pik3ip1 expression decreased with the increase in IL-21 production in T cells and that the ability of T cells to produce IL-21 was significantly

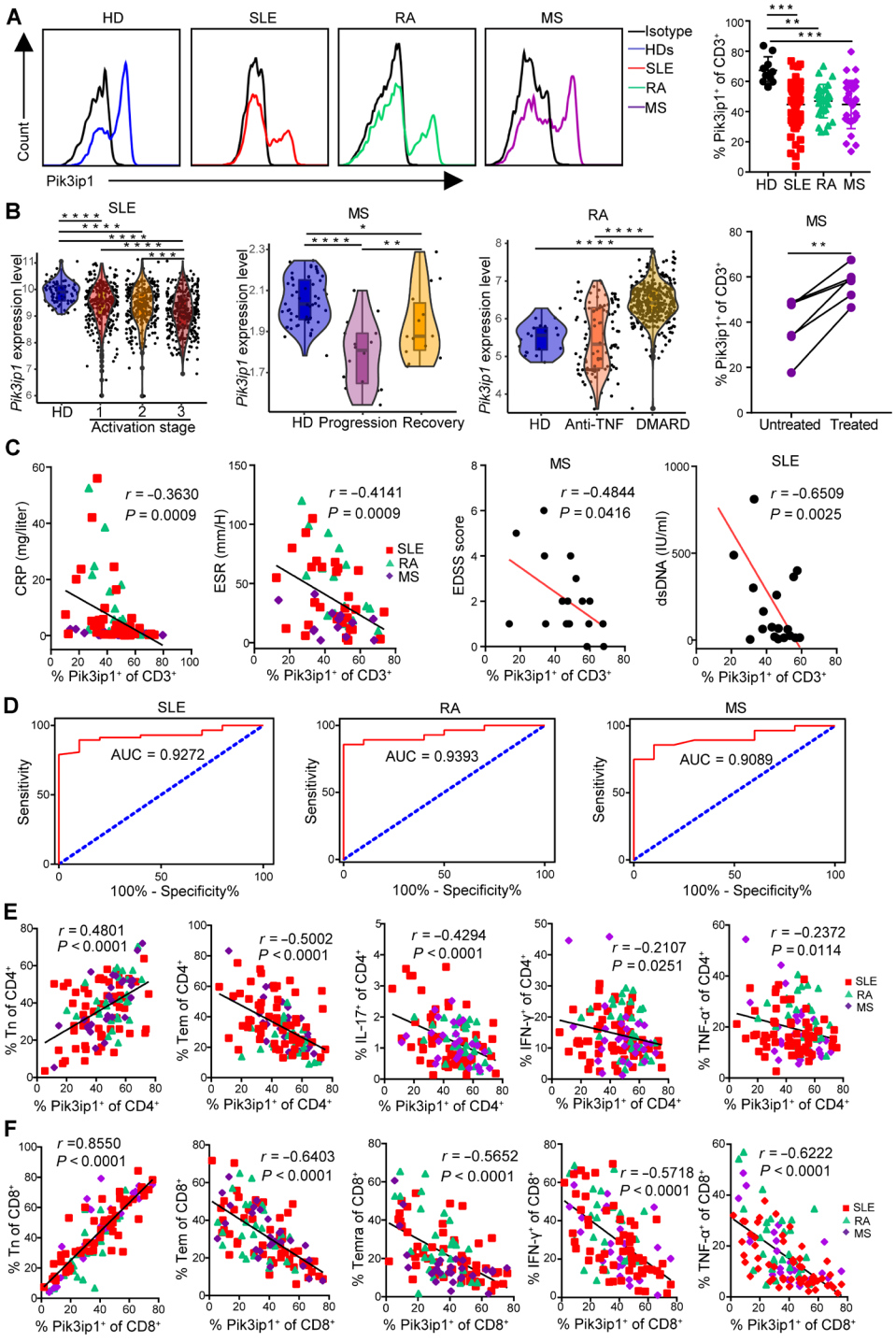

Fig. 1. Down-regulation of Pik3ip1 in multiple autoimmune diseases is associated with more severe clinical disease, poor treatment response, and altered T cell homeostasis. (**A**) Flow cytometry analysis showing the down-regulation of Pik3ip1 expression in $CD3^+$ T cells in PBMC from patients with SLE ($n = 57$), RA ($n = 28$), and MS ($n = 28$) compared to HDs ($n = 10$). (**B**) Violin plots showing the reduction in Pik3ip1 expression as SLE progresses, the increased expression of Pik3ip1 in patients with MS at recovery stage, and the higher level of Pik3ip1 expression after DMARD treatment in patients with RA compared with placebo and anti-TNF treatment groups, respectively. The above cohorts were derived from RNA-seq datasets in the Gene Expression Omnibus database. Flow cytometry analysis showing the up-regulation of Pik3ip1 expression in $CD3^+$ T cells in PBMC from patients with MS ($n = 6$) after treatment. (**C**) Correlation between the percentage of $Pik3ip1^+$ $CD3^+$ T cells with serum CRP and ESR levels in patients with SLE, RA, and MS; disease severity score in patients with MS; and anti-dsDNA antibody in a patient with SLE. (**D**) The ROC curves of Pik3ip1 expression to validate its potential diagnostic value in SLE, RA, and MS. (**E** and **F**) Correlation between the percentage of $Pik3ip1^+$ $CD4^+$ (E) or $CD8^+$ (F) T cells with the percentages of naïve T cell (Tn), effector memory T cell (Tem), Temra, IL-17–producing, IFN-γ–producing, and TNF-α–producing T cell subsets in PBMC from patients with SLE, RA, and MS. Data are shown as means ± SEM. Each data point represents an individual subject. Differences between groups are analyzed by Student's *t* test or one-way analysis of variance (ANOVA) test. $^*P < 0.05$; $^{**}P < 0.01$; $^{***}P < 0.001$; $^{****}P < 0.0001$.

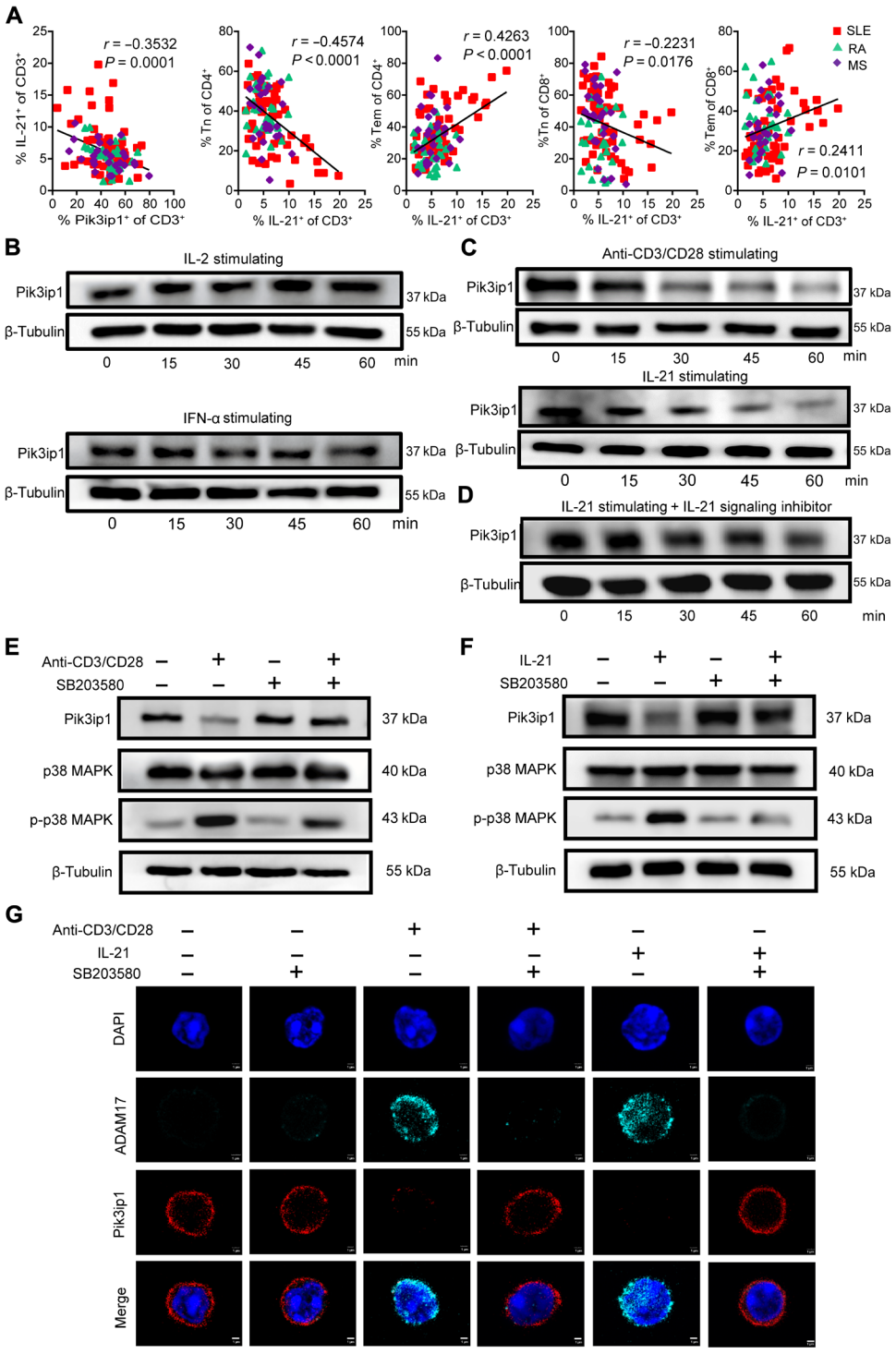

Fig. 2. IL-21 stimulation reduces the expression of Pik3ip1 by activating MAPK and up-regulating ADAM17 in T cells. (**A**) Correlations between the percentage of IL-21–producing T cells with the percentages of Pik3ip1$^+$ T cells and Tn and Tem subsets in CD4$^+$ or CD8$^+$ T cell compartments in PBMC from patients with SLE ($n = 57$), RA ($n = 28$), and MS ($n = 28$). (**B**) Pik3ip1 protein level in CD3$^+$ T cells derived from wild-type mice after IL-2 (20 U/ml) or IFN-α (500 U/ml) stimulation was analyzed by Western blot every 15 min. (**C**) Pik3ip1 protein level in CD3$^+$ T cells derived from wild-type mice after anti-CD3/CD28 (3 μg/ml) or IL-21 (300 ng/ml) stimulation was analyzed by Western blot every 15 min. (**D**) Pik3ip1 protein level in CD3$^+$ T cells derived from wild-type mice after IL-21 (300 ng/ml) stimulation and 1000 nM tofacitinib treatment was analyzed by Western blot every 15 min. (**E** and **F**) The protein expression of Pik3ip1, p38 MAPK, and p-p38 MAPK in CD3$^+$ T cells derived from wild-type mice treated with or without SB203580 (p38 MAPK inhibitor) after anti-CD3/CD28 (E) or IL-21 (F) stimulation was analyzed by Western blot. (**G**) Confocal microscopy analysis of Pik3ip1 and ADAM17 expression in CD3$^+$ T cells derived from wild-type mice. CD3$^+$ T cells were administrated or not with SB203580 (20 μM), a selective p38 MAPK inhibitor, under the stimulation of anti-CD3/CD28 (3 μg/ml) or IL-21 (300 ng/ml) or no stimulation for 1 hour. Scale bars, 1 μm. Data in (B) to (G) are from three independent experiments with similar results. Each data point represents an individual subject. DAPI, 4′,6-diamidino-2-phenylindole.

related to T cell activation (Fig. 2A). Up-regulation of IL-21 level has been detected in the peripheral blood and tissues of patients with multiple autoimmune diseases (*26*). To further explore the role of IL-21 in the regulation of Pik3ip1 expression, we performed in vitro stimulation using splenic T cells exposure to several inflammatory cytokines. Our results revealed that IL-2 or IFN-α stimulation alone had no effect on Pik3ip1 expression in T cells in vitro (Fig. 2B). However, we found a notable reduction in Pik3ip1 expression in the IL-21–simulated model, which was similar to those observed under the anti-CD3/CD28 stimulation, and a marked recovery in the presence of tofacitinib, an IL-21 signaling inhibitor (Fig. 2, C and D) (*27*). Furthermore, we found that the protein expressions of both p38 MAPK and p-p38 MAPK in T cells showed an up-regulation after stimulation, and the loss of Pik3ip1 protein expression induced by either anti-CD3/CD28 or IL-21 stimulation was markedly alleviated by SB203580, a selective p38 MAPK inhibitor (Fig. 2, E and F). Previous study has reported that ADAM17 acts as a molecular scissor that proteolytically cleaves the extracellular domain of Pik3ip1, leading to a loss of Pik3ip1 on the cell surface (*16*). Consistently, we observed that contrary to Pik3ip1, ADAM17 increased its expression after stimulation and this alteration was reversed through SB203580 administration (Fig. 2G), highlighting the role of p38 MAPK in ADAM17-mediated Pik3ip1 reduction. These results indicate that excessive IL-21 production in the autoimmune environment is at least partially responsible for the decreased Pik3ip1 in a p38 MAPK–dependent manner.

Pik3ip1 deficiency in T cells exacerbates experimental autoimmune encephalomyelitis

To investigate the role of Pik3ip1 in autoimmune diseases, we constructed $CD4^{Cre}$*Pik3ip1*$^{flox/flox}$ mice [conditional knockout (cKO)] with Pik3ip1-specific KO on T cells. We found that the deletion of Pik3ip1 did not detectably affect T cell development in the thymus, evidenced by the comparable frequencies of $CD4^-$ $CD8^-$, $CD4^+$ $CD8^-$, $CD8^+$ $CD4^-$, and $CD4^+$ $CD8^+$ thymic T cells between control and cKO mice at young (2 months) and aged (6 months) mice (fig. S2A). Meanwhile, there was no significant difference in the activation status of thymic T cells between cKO mice and control mice at different ages (fig. S2B). In the periphery, we also noticed that the distribution of splenic T cells in Tn ($CD44^-$ $CD62L^+$) and Tem ($CD44^+$ $CD62L^-$) subsets differed only slightly in the $CD8^+$ compartment (fig. S2C), suggesting that genetical KO of Pik3ip1 had minimal impact on T cell peripheral homeostasis. Next, we tested the effects of genetic Pik3ip1 disruption in T cells from cKO mice on the experimental autoimmune encephalomyelitis (EAE) model, the most commonly used animal model for MS, to further investigate the cause-effect relationship between Pik3ip1 expression and autoimmune pathology (Fig. 3A). As expected, we found that cKO mice exhibited a more severe course of EAE than the control mice, characterized by a significant increase in the clinical score (Fig. 3B). Furthermore, EAE is an autoimmune disease characterized by chronic inflammatory demyelinating lesions in the central nervous system (CNS) and the infiltration of activated T helper 1 (T_H1) and T_H17 cells is thought to play a central role in CNS inflammation and disease pathogenesis (*28*). We therefore examined the number of infiltrated T cell subsets in the CNS and spleen of these two groups after immunization. We found that cKO mice yielded more $CD4^+$ T cells, T_H1, T_H17, and $CD8^+$ T cells in the CNS and spleen compared to control mice (Fig. 3C). We also examined the sections of the brain and spinal cord from these two groups by hematoxylin and eosin (HE) staining. Consistently, we observed far more inflammatory foci in the cKO mice than in the control group (Fig. 3D).

We next compared T cell activation status and the production of proinflammatory cytokines between these two groups during EAE. We observed that the frequency of CNS and splenic T cells exhibiting Tem phenotype was higher in the cKO mice compared with the control mice. Correspondingly, the frequency of CNS and splenic T cells exhibiting Tn phenotype was lower in the cKO mice compared with the control mice (Fig. 3E and fig. S2D). Furthermore, the proportions of IL-17–producing and IFN-γ–producing $CD4^+$ T cells in the CNS and spleen were significantly higher in the cKO mice than in the control mice (Fig. 3, F and G). In addition, we observed a higher frequency of TNF-α– and IL-2–producing T cells and IFN-γ–producing $CD8^+$ T cells in the CNS of the cKO mice compared with the control mice, whereas there was no statistical difference in the spleen (Fig. 3, H and I, and fig. S2, E to G). These data suggest that Pik3ip1 deficiency leads to a skewed differentiation of T cells toward proinflammatory T cell subsets, which contribute to unleash autoimmune responses and promote immunopathology.

The hyperactive phenotype of T cells with Pik3ip1 depletion results from reduced OXPHOS and increased glycolysis

To illustrate the underlying mechanisms of Pik3ip1 in T cell activation and function, we sorted paired $Pik3ip1^+$ T cells and $Pik3ip1^-$ T cells from the spleen of naïve wild-type mice for bulk RNA-seq. It was apparent that $Pik3ip1^+$ T cells exhibited a distinct transcriptional profile that was largely dissimilar from $Pik3ip1^-$ T cells, as they mapped far from each other along the first principal component (PC1) (Fig. 4A and fig. S3, A and B). Consistently, we found that $Pik3ip1^-$ T cells up-regulated activation-related genes while down-regulating the quiescence-related genes. Notably, pronounced changes were observed in genes contributed to metabolic regulation with a significant down-regulation of genes involved in OXPHOS and up-regulation of genes involved in glycolysis in $Pik3ip1^-$ T cells (Fig. 4B). Gene set enrichment analysis (GSEA) from the differential genes down-regulated in $Pik3ip1^-$ T cells also showed enrichment for OXPHOS and mitochondrial electron transport pathways, while the differential genes up-regulated in $Pik3ip1^-$ T cells were enriched of immune effector and cytokine signaling pathways (Fig. 4C and fig. S3C). These results suggest a strong relationship between Pik3ip1 expression and metabolic reprogramming in T cells.

To further demonstrate the role of Pik3ip1 in T cell metabolic homeostasis, we sorted $CD4^+$ and $CD8^+$ T cells from the spleen of control or cKO mice to assess their metabolic functions by performing a seahorse mitochondrial stress test and glycolysis stress test. Oxygen consumption rate (OCR) and extracellular acidification rate (ECAR) were measured for mitochondrial respiration and glycolysis, respectively. We found that the basal OCR, maximal respiration, spare respiratory capacity, and adenosine 5′-triphosphate (ATP) production of cKO T cells were lower than that of control T cells (Fig. 4D). In contrast, cKO T cells exhibited increased ECAR compared to control T cells, which was evident with increased glycolytic capacity and reserve in cKO T cells (Fig. 4E).

Mitochondria are thought to be the main place of OXPHOS and cellular ATP production. We next investigated whether the reduced OXPHOS in Pik3ip1-deficient T cells was attributed to impaired mitochondrial function. $CD4^+$ and $CD8^+$ T cells isolated from the spleen of control or cKO mice were stained with tetramethylrhodamine methyl ester (TMRM), a cell-permeant and fluorescent

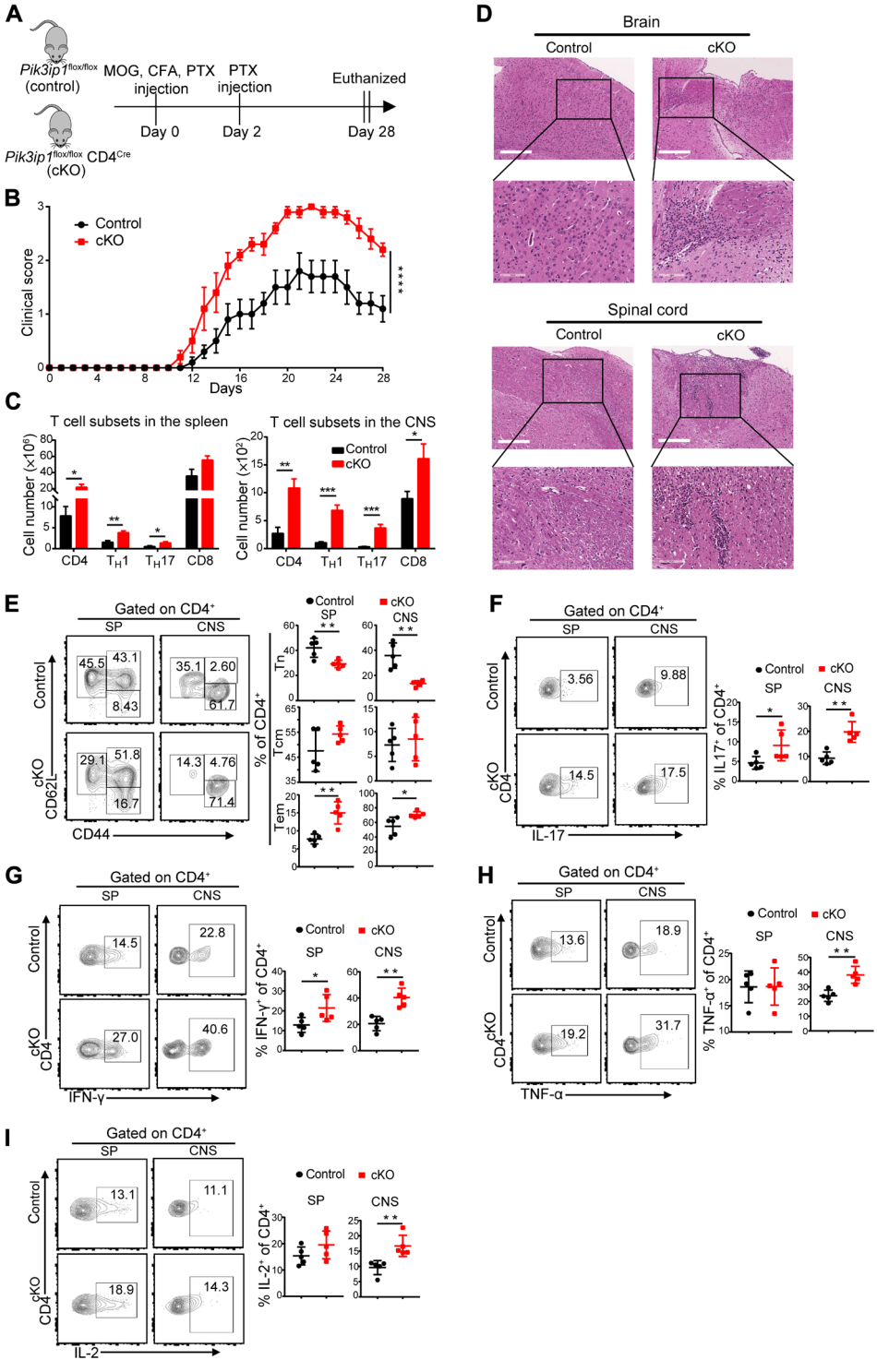

Fig. 3. Pik3ip1 deficiency in T cells results in exacerbated EAE. (**A**) Induction of EAE in control and cKO mice ($n = 5$ mice per group). (**B**) The severity of EAE was evaluated daily using an EAE clinical score. (**C**) Quantification of T cell subsets in the spleen (SP) and the CNS from control and cKO mice. (**D**) Histological analysis of brain and spinal cord in control and cKO mice. Scale bars, 300 μm (top) and 100 μm (bottom). (**E**) Activation status of $CD4^+$ T cells in the CNS and spleen of control and cKO mice assessed by CD44 and CD62L expression. (**F** to **I**) The percentages of IL-17–producing (F), IFN-γ–producing (G), TNF-α–producing (H), and IL-2–producing (I) $CD4^+$ T cells in the CNS and spleen of control and cKO mice are shown. Data are presented as the means ± SEM from three independent experiments. Each dot represents an individual mouse. Differences between groups are analyzed by repeated-measures ANOVA or Student's *t* test. $^*P < 0.05$; $^{**}P < 0.01$; $^{***}P < 0.001$; $^{****}P < 0.0001$.

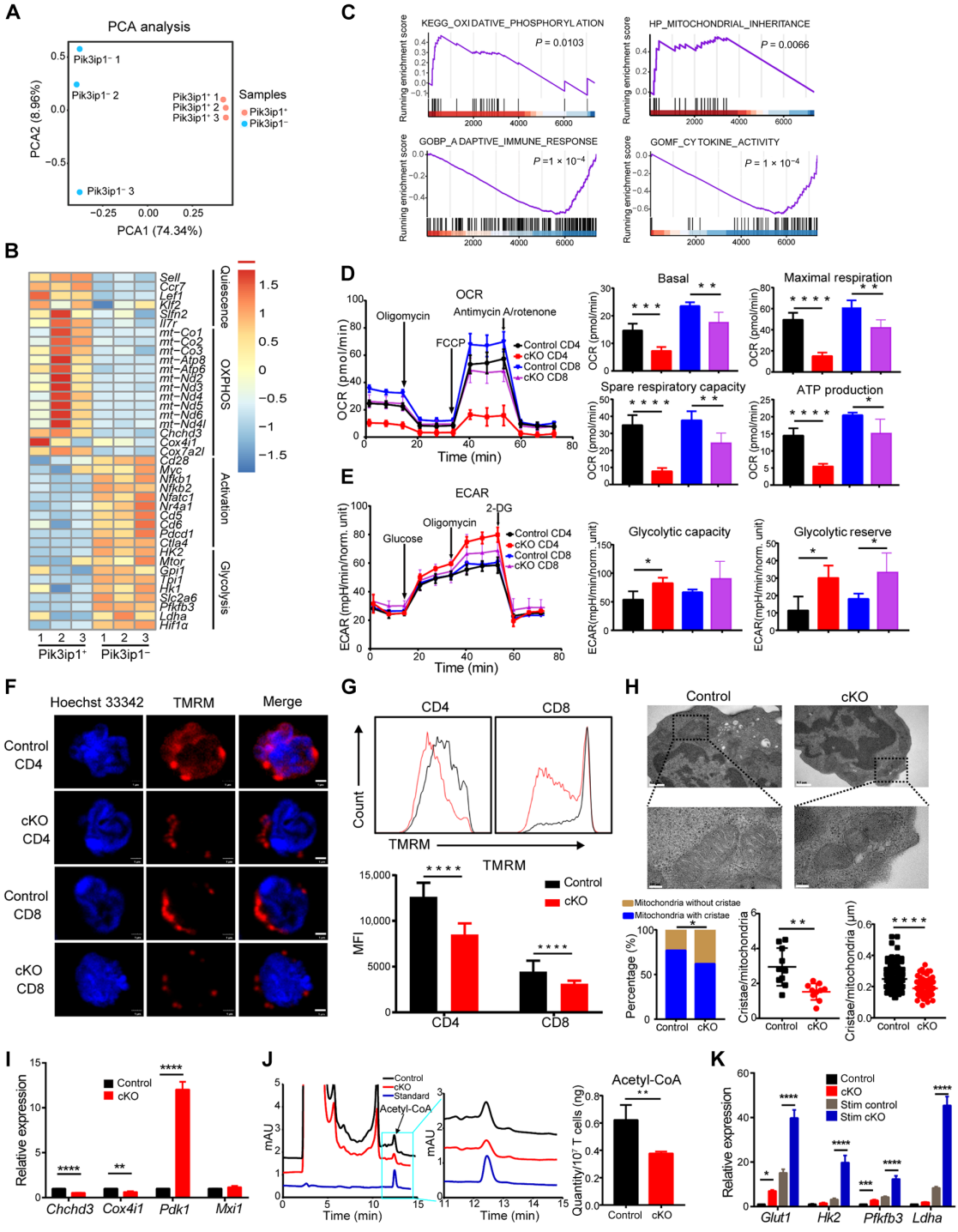

Fig. 4. Pik3ip1 ablation reduces OXPHOS but increases glycolysis in T cells. (**A**) PCA of Pik3ip1$^+$ and Pik3ip1$^-$ T cells for their gene expression patterns. (**B**) Heatmap showing the expression level of select genes in each sample. (**C**) GSEA showing pathways enriched in Pik3ip1$^+$ and Pik3ip1$^-$ T cells. (**D**) OCR of control and cKO CD4$^+$ and CD8$^+$ T cells and bar plots showing basal OCR, maximal OCR, spare respiratory capacity, and ATP production. (**E**) ECAR of control and cKO CD4$^+$ and CD8$^+$ T cells and bar plots showing glycolytic capacity and glycolytic reserve. (**F**) Representative confocal microscopic images of control and cKO CD4$^+$ and CD8$^+$ T cells after TMRM staining. Scale bars, 1 μm. (**G**) Flow cytometry analyses of CD4$^+$ and CD8$^+$ T cell mitochondrial membrane potential measured by TMRM fluorescence intensity. (**H**) Representative transmission electron microscope images showing mitochondria area in control and cKO CD3$^+$ T cells at two different magnifications (top) and statistics regarding the cristae in each mitochondrion (bottom). Scale bars, 0.5 μm (top) and 100 nm (bottom). (**I**) RT-qPCR analyses of *Chchd3*, *Cox4i1*, *Pdk1*, and *Mxi1* expression in control and cKO CD3$^+$ T cells. (**J**) Liquid chromatography results of the acetyl-CoA level in control and cKO CD3$^+$ T cells. mAU, milli–absorbance units. (**K**) RT-qPCR analyses of *Glut1*, *Hk2*, *Pfkfb3*, and *Ldha* expression in control, cKO, Stim control, and Stim cKO CD3$^+$ T cells. Stim, purified T cells that were stimulated with anti-CD3/CD28 antibody (3 μg/ml) for 4 hours. Data are presented as the means ± SEM from three independent experiments. Data in RT-qPCR analysis are normalized to control T cells. Differences between groups are analyzed by unpaired Student's *t* test. *$P < 0.05$; ** $P < 0.01$; *** $P < 0.001$; **** $P < 0.0001$.

dye for labeling active mitochondria. We observed a significant decrease in mitochondrial membrane potential in cKO T cells as compared to control T cells, measured by the fluorescence intensity of TMRM using both fluorescence microscopy (Fig. 4F) and flow cytometry (Fig. 4G). Consistently, a larger proportion of mitochondria without cristae was found in cKO T cells compared to control T cells. The number and length of cristae in each mitochondrion were also significantly reduced in cKO T cells in comparison with control T cells (Fig. 4H).

We next dissected the transcriptional profile of T cells after Pik3ip1 deficiency using real-time quantitative polymerase chain reaction (RT-qPCR). Consistently, our results showed that the expression of key OXPHOS genes, such as *Chchd3* and *Cox4i1*, was decreased in cKO T cells compared to control T cells. In contrast, the expression of *Pdk1*, an important regulator of the mitochondrial enzyme pyruvate dehydrogenase, which is responsible for the conversion of pyruvate to acetyl–coenzyme A (CoA), was significantly higher in cKO T cells when compared to control T cells (Fig. 4I). In support of this, the level of acetyl-CoA in cKO T cells was shown to be significantly lower than that in control T cells (Fig. 4J). On the other hand, glycolysis-related molecules *Glut1*, *Pfkfb3*, *Hk2*, and *Ldha* were found to up-regulate their expression in cKO T cells compared to control T cells. These increases were more pronounced in T cells after stimulation (Fig. 4K).

Metabolic adaptation toward aerobic glycolysis is one of the hallmarks of T cell quiescence exit (*29*). To address the importance of metabolic reprogramming in the activation-poised state of Pik3ip1-deficient T cells, we measured the activation status and cytokine production of T cells from cKO mice after treatment with 2-deoxy-D-glucose (2-DG) or AZ33, both of which are glycolysis inhibitors. In support of our assumptions, 2-DG or AZ33 treatment markedly suppressed the aberrant T cell activation and increased the production of proinflammatory cytokines that resulted from Pik3ip1 deficiency to the levels even similar to those seen in T cells from control mice (Fig. 5, A to D, and fig. S3, D and E). Collectively, these findings strongly indicate that the ablation of Pik3ip1 could induce T cell metabolic shift from OXPHOS to glycolysis, thereby leading to a poised state for activation.

Hif1α is required for the metabolic reprogramming in T cells with Pik3ip1 deletion

We have shown that cKO T cells have reduced OXPHOS while enhancing glycolysis compared to control T cells. We then aimed to address the molecular mechanisms that drive this metabolic reprogramming. Using bulk RNA-seq, we demonstrated a significant increase in the expression of several previously reported reprogramming mediators in Pik3ip1^{-} T cells, such as *Hif1α*, Myc proto-oncogene (*Myc*), *Irf4*, and high-mobility group box 1 (*Hmgb1*) (Fig. 6, A and B) (*30*–*33*). Among these, *Hif1α* tended to exhibit the largest magnitude (Fig. 6C). Furthermore, in patients with SLE, RA, MS, SS, or systemic juvenile idiopathic arthritis (SJIA), the expression of Hif1α was significantly inversely correlated with Pik3ip1 expression in T cells, indicating that Hif1α is also likely to be negatively affected by the expression level of Pik3ip1 under autoimmune condition (Fig. 6D and fig. S4A). As mentioned previously, Pik3ip1 acts as an inhibitor of PI3K–Akt–mammalian target of rapamycin (mTOR) pathway, and it has been demonstrated that there is a strong link between Hif1α and mTOR signaling (*34*). To better understand the relationship between Pik3ip1 and Hif1α, we analyzed the Hif1α expression in the presence or absence of rapamycin, a specific mTOR inhibitor, in control and cKO T cells. As expected, the protein level of Hif1α and PI3K-Akt-mTOR pathway molecules was markedly up-regulated in cKO T cells compared with control T cells (Fig. 6E). However, the increase observed in cKO T cells was markedly reduced after rapamycin administration to the level even lower to that observed in control T cells, demonstrating a direct regulatory role of Pik3ip1 in Hif1α expression mediated by mTOR signaling (Fig. 6F). Hence, we postulated that Hif1α might play an essential role in the metabolic reprogramming that resulted from Pik3ip1 deficiency.

To test this hypothesis, we assessed the metabolic activities in control and cKO T cells using the Hif1α inhibitor, BAY87-2243 (*35*, *36*). TMRM analysis revealed complete recovery of the severely dampened mitochondrial membrane potential in cKO T cells in the presence of BAY87-2243 (Fig. 6, G and H, and fig. S4, B and C). Furthermore, we found that the difference in the expression of mitochondrial genes *Pdk1* between control and cKO T cells observed in our RT-qPCR studies disappeared after BAY87-2243 administration (Fig. 6I), suggesting that the reduced OXPHOS in cKO T cells after Pik3ip1 deletion primarily relies on the up-regulation of Hif1α/pyruvate dehydrogenase kinase 1 (Pdk1) axis. On the other hand, the increase in *Hif1α* and glycolysis-related genes *Glut1*, *Hk2*, *Pfkfb3*, and *Ldha* was attenuated as evidenced by similar levels between control and cKO + BAY87-2243 group (Fig. 6J). Moreover, we found that the cKO T cells showed more lactate acid accumulation compared with control T cells, which could be explained by the elevated glycolysis in cKO T cells, as lactate acid is an end product of glycolysis. As expected, BAY87-2243 treatment could partially abolish the effects of Pik3ip1 deficiency on lactate secretion in T cells (Fig. 6K).

We next explored the impacts of Hif1α inhibition on the T cell activation status and cytokine production by T cells after Pik3ip1 depletion in vitro. As our results indicated, compared to control T cells, cKO T cells were shown to have larger proportion of Tem while having smaller proportion of Tns and produced more proinflammatory cytokines upon activation. We also demonstrated that the ability of Hif1α inhibitor and rapamycin to reduce this hyperactive phenotype of cKO T cells was evident, with a reduction to proinflammatory cell proportions similar to that of control T cells (Fig. 7, A and B, and fig. S4, D and E). Together, these findings suggest that the elevated Hif1α is indispensable for the metabolic reprogramming toward glycolysis in Pik3ip1-deficient T cells and Hif1α inhibition acts as an effective strategy against this alteration, thus reversing the proinflammatory T cell phenotype after Pik3ip1 depletion.

Hif1α inhibition effectively reduces the increased EAE severity in Pik3ip1-deficient mice

To further explore the role of Pik3ip1/Hif1α/glycolysis axis in the autoimmune setting, we performed the EAE model as described above on three groups of mice, including control, cKO, and cKO + BAY87-2243 (Fig. 8A). We found that the clinical score decreased markedly in cKO + BAY87-2243 mice compared to cKO mice, suggesting that the administration of Hif1α inhibitor on cKO mice could largely mitigate the clinical disease (Fig. 8B). In addition, the number of CD4^{+} T cells, T_H1, T_H17, and CD8^{+} T cells that infiltrated in the cKO + BAY87-2243 mice, particularly in the CNS of the cKO + BAY87-2243 mice, was significantly reduced to the level seen in the control group. However, despite that the Hif1α inhibitor showed a full inhibition effect in the CNS, it was not sufficient to

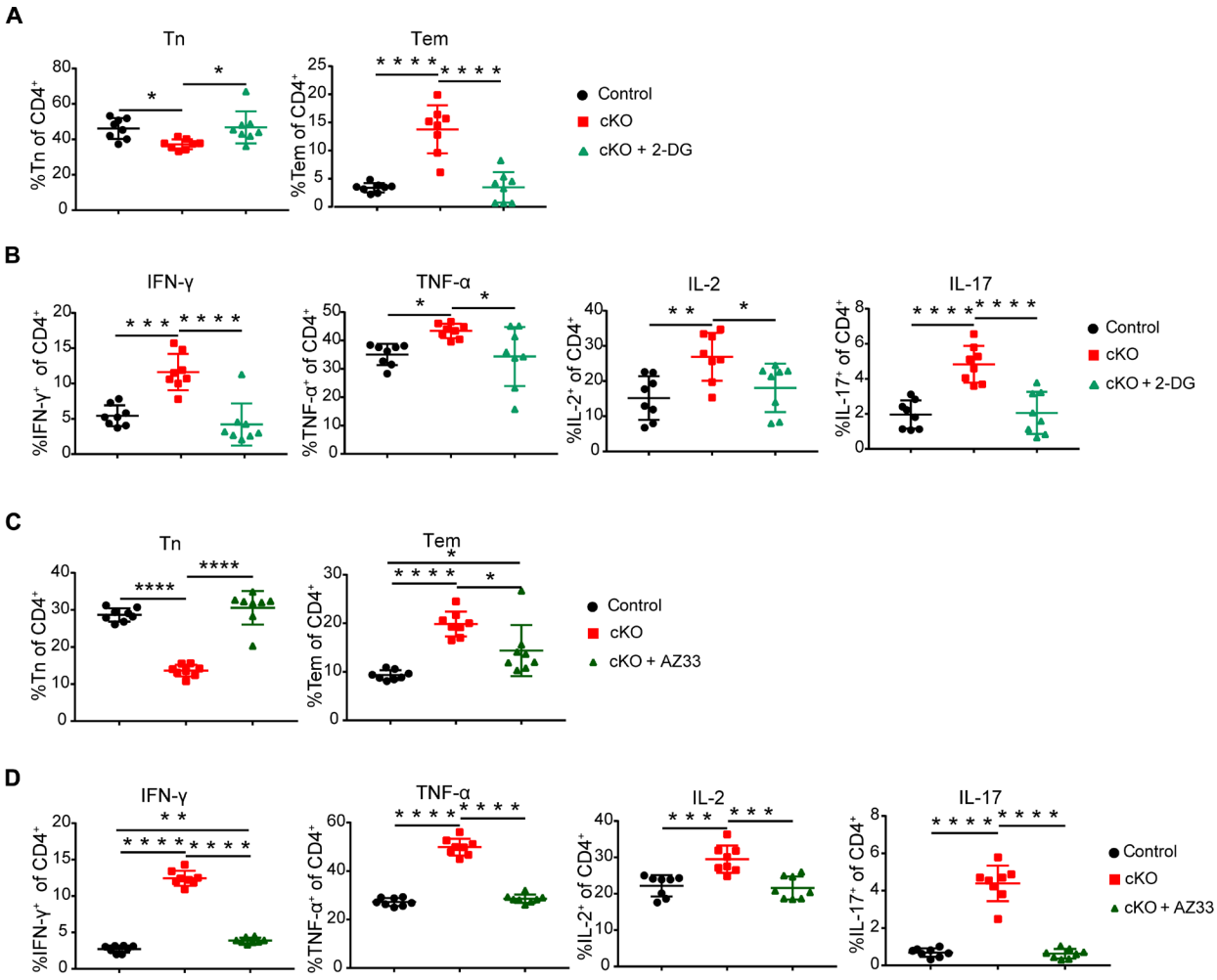

Fig. 5. Inhibition of glycolysis by 2-DG or AZ33 reversed the hyperactive phenotype of cKO T cells. (**A** and **B**) Activation status of $CD4^+$ T cells assessed by CD44 and CD62L expression (A) and the percentages of IL-17–, IFN-γ–, TNF-α–, and IL-2–producing $CD4^+$ T cells (B) in the spleen of control, cKO, and cKO + 2-DG (50 mM) mice are shown. (**C** and **D**) Activation status of $CD4^+$ T cells assessed by CD44 and CD62L expression (C) and the percentages of IL-17–, IFN-γ–, TNF-α–, and IL-2–producing $CD4^+$ T cells (D) in the spleen of control, cKO, and cKO + AZ33 (150 μM) mice are shown. Purified T cells (200,000 cells per well) were cultured with or without 2-DG and AZ33 in a 96-well flat-bottom plate coated with anti-CD3/CD28 antibody (1.5 μg/ml) for 72 hours before fluorescence-activated cell sorting (FACS) staining. Data are presented as the means ± SEM from three independent experiments. Differences between groups were analyzed by one-way ANOVA test. *$P < 0.05$; **$P < 0.01$; ***$P < 0.001$; ****$P < 0.0001$.

suppress T cell infiltration in the spleen (Fig. 8C). The reversal of inflammatory infiltration in EAE lesion has been found to be associated with improved disease prognosis (*37*). HE staining further demonstrated the reduced proinflammatory cells in the brain and spinal cord morphologically after BAY87-2243 treatment (Fig. 8D).

Likewise, to determine whether Hif1α inhibition could suppress the hyperactivity of T cells in autoimmune diseases, we compared the T cell activation status and cytokine production by T cells before and after BAY87-2243 treatment using the same EAE model. In the presence of BAY87-2243, the frequency of CNS T cells and splenic T cells exhibiting Tem phenotype in the cKO mice was reduced, whereas those exhibiting Tn phenotype showed an opposite trend (Fig. 8E and fig. S5A). Consistent with this, Hif1α inhibition was also able to reduce the production of IL-17, IFN-γ, and TNF-α by $CD4^+$ T cells in the CNS of the cKO mice. Note that the cytokine production by T cells in the spleen was not altered, suggesting a minimal effect on inflammatory response in the spleen (Fig. 8, F to H). However, no significant difference was detected between cKO and cKO + BAY87-2243 mice in the percentages of IFN-γ– or TNF-α–producing $CD8^+$ T cells and IL-2–producing T cells (Fig. 8I and fig. S5, B to D). In addition, we observed a significant reduction in T cell glycolysis in the spleen of the cKO mice following BAY87-2243 treatment as revealed by lactate acid production (Fig. 8J). These results indicate that the inhibition of Hif1α alleviates the increased EAE severity due to Pik3ip1 deficiency by restoring T cell metabolic homeostasis and reducing proinflammatory T cell infiltration.

DISCUSSION

Here, we unveil a previously unrecognized role of Pik3ip1, a negative immune regulator, in maintaining T cell metabolic homeostasis by coordinating the balance between OXPHOS and aerobic glycolysis through Hif1α. Our results have shown that, in autoimmune patients, consistent down-regulation of Pik3ip1 mediated by IL-21/p38 MAPK/ADAM17 pathway contributes to shifting the metabolic balance in favor of glycolysis, thereby promoting

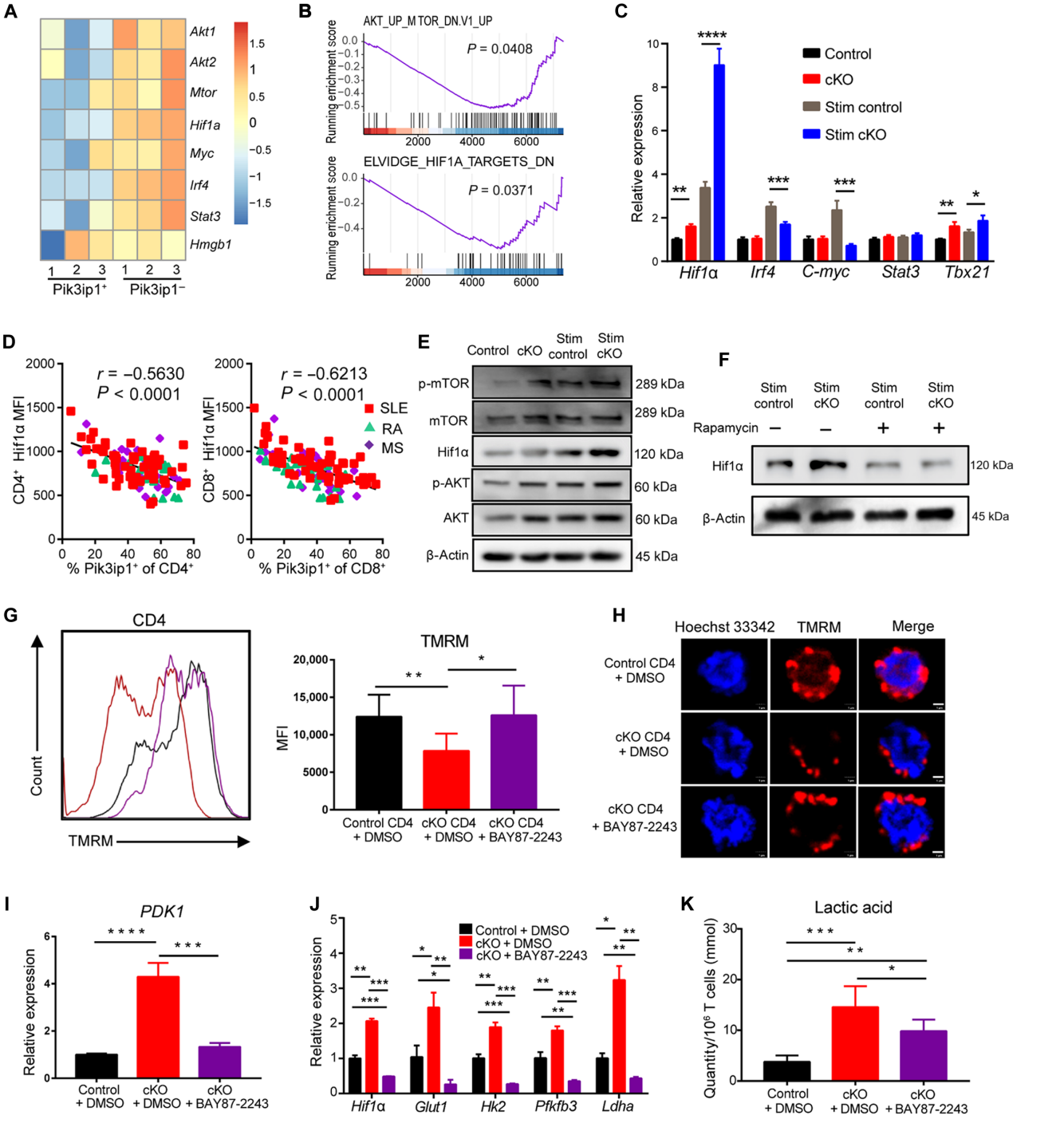

Fig. 6. Hif1α is responsible for the metabolic reprogramming in T cells with Pik3ip1 deficiency. (**A**) Heatmap showing the up-regulation of several metabolic reprogrammers in Pik3ip1$^+$ T cells compared with Pik3ip1$^-$ T cells at steady state. (**B**) GSEA results showing AKT up mTOR and Hif1α pathways enriched in Pik3ip1$^-$ T cells. (**C**) RT-qPCR of *Hif1α*, *Irf4*, *C-myc*, *Stat3*, and *Tbx21* expression in control, cKO, Stim control, and Stim cKO CD3$^+$ T cells. Stim, purified T cells that were cultured with anti-CD3/CD28 antibody (3 μg/ml) for 4 hours. (**D**) Correlation between the percentage of Pik3ip1$^+$ T cells with the MFI of Hif1a in T cells from patients with SLE, RA, and MS. (**E**) Representative immunoblots of p-mTOR, mTOR, Hif1α, p-AKT, AKT, and β-actin in control, cKO, Stim control, and Stim cKO CD3$^+$ T cells. (**F**) Representative immunoblots of Hif1α and β-actin in Stim control, Stim cKO, Stim control + rapamycin (mTOR inhibitor, 10 nM), and Stim cKO + rapamycin CD3$^+$ T cells. (**G**) Flow cytometry analyses of control, cKO, and cKO + BAY87-2243 (Hif1a inhibitor, 1 μM) CD4$^+$ T cell mitochondrial membrane potential measured by TMRM fluorescence intensity. (**H**) Representative confocal microscopic images of control, cKO, and cKO + BAY87-2243 CD4$^+$ T cells after TMRM staining. DMSO, dimethyl sulfoxide. Scale bars, 1 μm. (**I** and **J**) RT-qPCR analyses of *Pdk1* (I), *Hif1α*, *Glut1*, *Hk2*, *Pfkfb3*, and *Ldha* expression (J) in control, cKO, and cKO + BAY87-2243 CD3$^+$ T cells. (**K**) Lactate acid level in control, cKO, and cKO + BAY87-2243 (1 μM) CD3$^+$ T cells was assessed before a 4-hour stimulation using anti-CD3/CD28 antibody (3 μg/ml). Data are presented as means ± SEM from three independent experiments. Each data point represents an individual subject. Differences between groups are analyzed by unpaired Student's *t* test or one-way ANOVA test. **P* < 0.05; ***P* < 0.01; ****P* < 0.001; *****P* < 0.0001.

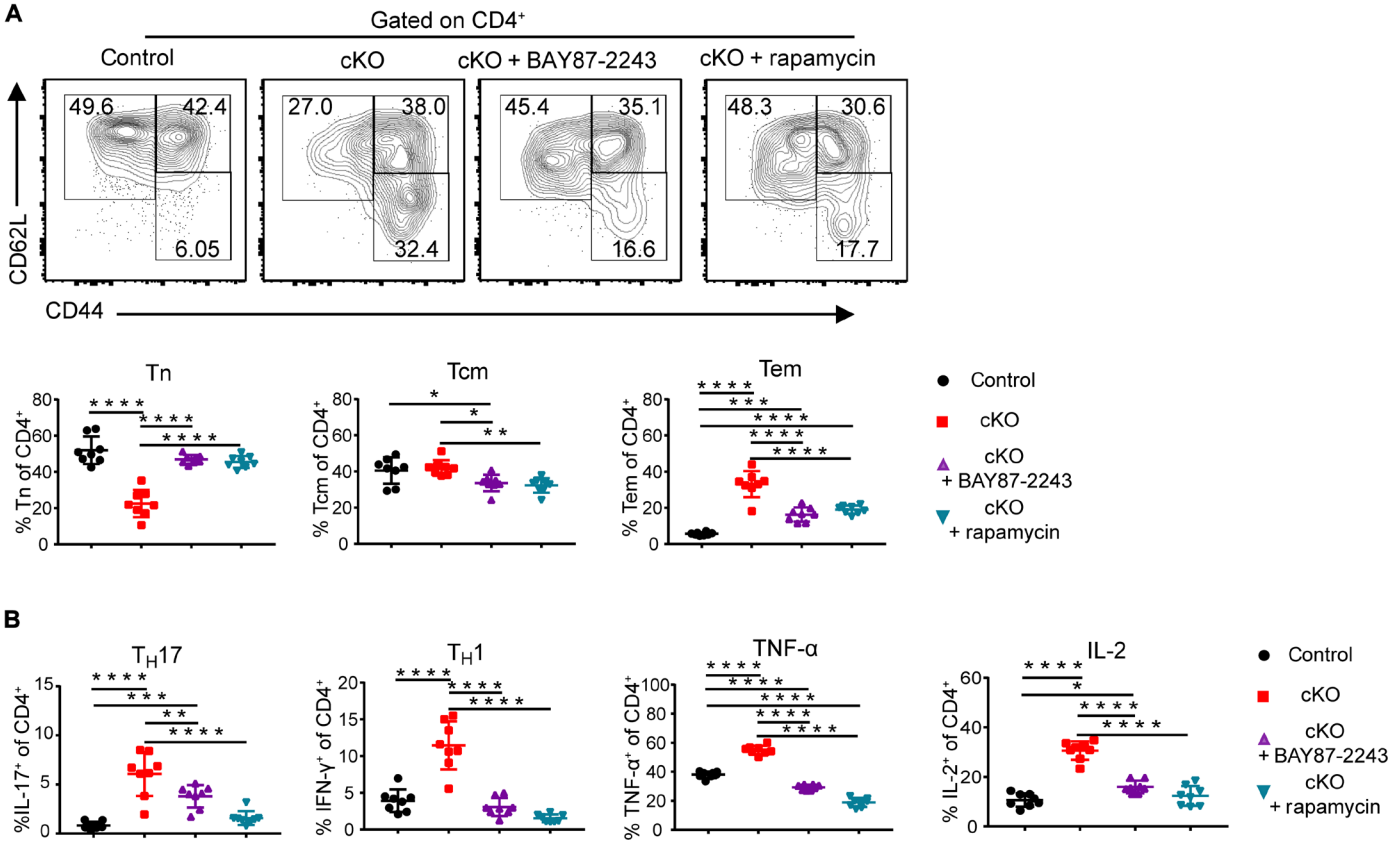

Fig. 7. Inhibition of Hif1α or mTOR reduces the hyperactive phenotype of cKO T cells. (**A**) Activation status of $CD4^+$ T cells in the spleen of control, cKO, cKO + BAY87-2243 (1 μM), and cKO + rapamycin (10 nM) mice assessed by CD44 and CD62L expression. (**B**) The percentages of IL-17-producing, IFN-γ–, TNF-α–, and IL-2–producing $CD4^+$ T cells in the spleen of control, cKO, cKO + BAY87-2243 (1 μM), and cKO + rapamycin (10 nM) mice are shown. Purified T cells (200,000 cells per well) were cultured with or without BAY87-2243 and rapamycin in a 96-well flat-bottom plate coated with anti-CD3/CD28 antibody (1.5 μg/ml) for 72 hours before FACS staining. Data are presented as means ± SEM from three independent experiments. One-way ANOVA analysis was performed to compare control, cKO, cKO + BAY87-2243, and cKO + rapamycin groups. *$P < 0.05$; **$P < 0.01$; ***$P < 0.001$; ****$P < 0.0001$.

proinflammatory activation of T cells. Lower expression level of Pik3ip1 in T cells also indicates more severe disease and worse treatment response. Our study proposes that targeting Pik3ip1/Hif1a/glycolysis axis could be investigated as a potential therapeutic strategy for autoimmune diseases.

Despite the success of exploiting negative immune regulators in tumor immunotherapy, therapeutics that directly target negative immune regulators in autoimmunity are limited and display an increased risk of infection and tumor (*38*). We have shown here that Pik3ip1, a negative immune regulator, suppresses proinflammatory activation of T cells under multiple autoimmune conditions, providing a promising therapeutic target without any risk of protumorigenicity, as Pik3ip1 is also a negative regulator of PI3K and has been reported to inhibit the development of hepatocellular carcinoma (*15*). Furthermore, Pik3ip1 has been demonstrated to exert its function by distinct mechanisms. Unlike most negative immune regulators, which primarily function in activated T cells and tend to up-regulate their expression to inhibit excessive T cell activation during autoimmunity (*19*, *20*), Pik3ip1 showed significant loss in T cells from patients with SLE, RA, or MS. It is tempting to speculate that Pik3ip1 shows substantial impacts on the regulation of early T cell activation and the profound down-regulation of Pik3ip1 in the autoimmune setting lowers the threshold for T cells to activate when encounter self-antigens, thus accelerating the onset of autoimmunity. Consistently, in the murine EAE model, genetical depletion of Pik3ip1 in T cells could significantly worsen the disease progression. Note that *Pik3ip1* cKO mice under steady state develop no discernable sign of autoimmune diseases, suggesting that the absence of Pik3ip1 per se is not sufficient to initiate spontaneous autoimmunity. These observations were similar to those seen in mice depleted of T cell immunoreceptor with Ig and ITIM domains (TIGIT) or LAG-3 but in contrast to mice with single PD-1 or CTLA-4 depletion, which displayed autoimmune-like manifestations at steady state (*39*–*42*).

T cells exhibit distinct metabolic activity from other somatic cells and metabolic plasticity across different stages of differentiation, which provides the rationale for selectively modulating the metabolism of hyperactive T cells in the treatment of autoimmune diseases (*43*). It is known that up-regulation of glycolysis is a major feature of hyperactive T cells under autoimmune conditions (*44*). In the light of this, many glycolytic determinants of great therapeutic potential have been found. Previous studies have shown that the inhibition of critical molecules involved in glycolysis, such as glucose transporter 1 (Glut1), 6-phosphofructo-2-kinase/fructose-2,6-biphosphatase 3 (Pfkfb3), hexokinase 2 (Hk2), and lactate dehydrogenase A (Ldha), could attenuate the development of autoimmunity in multiple mice models including SLE, psoriasis, autoimmune arthritis, and a lethal

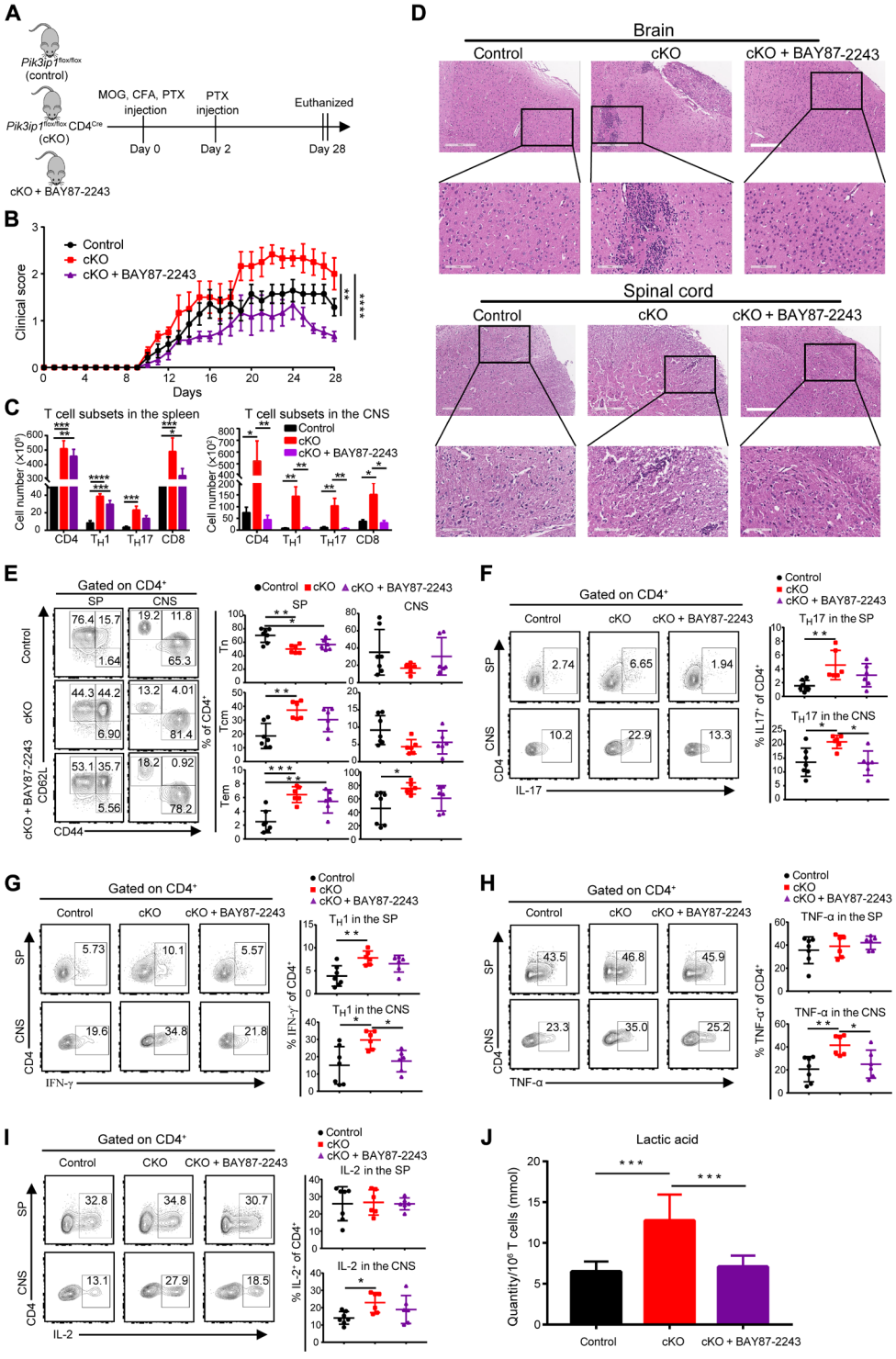

Fig. 8. Hif1α inhibition effectively reduces the increased EAE severity in Pik3ip1-deficient mice. (**A**) Induction of EAE in control, cKO and cKO + BAY87-2243 (4 mg/kg per day by gavage) mice ($n = 6$ or 7 mice per group). CFA, complete Freund's adjuvant; PTX, pertussis toxin. (**B**) The severity of EAE was evaluated daily using an EAE clinical score. Statistical analysis was performed using repeated-measures ANOVA. (**C**) Quantification of T cell subsets in the spleen and CNS from control, cKO, and cKO + BAY87-2243 mice. (**D**) Histological analysis of the brain and spinal cord in control, cKO, and cKO + BAY87-2243 mice. Scale bars, 300 μm (top) and 100 μm (bottom). (**E**) Activation status of $CD4^+$ T cells in the CNS and spleen of control, cKO, and cKO + BAY87-2243 mice assessed by CD44 and CD62L expression. (**F** to **I**) The percentages of IL-17–producing (F), IFN-γ–producing (G), TNF-α–producing (H), and IL-2–producing (I) $CD4^+$ T cells in the CNS and spleen of control, cKO, and cKO + BAY87-2243 mice are shown. (**J**) Lactate acid level in control, cKO, and cKO + BAY87-2243 T cells. One-way ANOVA with Bonferroni's multiple comparison was performed. Data are presented as means ± SEM from three independent experiments. Each dot represents an individual mouse. Differences between groups are analyzed by repeated-measures ANOVA or one-way ANOVA analysis. *$P < 0.05$; **$P < 0.01$; ***$P < 0.001$; ****$P < 0.0001$.

autoinflammatory condition (*9*, *45*–*48*). However, glycolysis-associated molecules are expressed widely throughout the body, and hence, directly targeting those proteins may result in an inevitable off-target side effect. In this study, we identified Pik3ip1 as a key metabolic regulator specifically in T cells, possibly providing a more effective therapeutic strategy in a wide range of autoimmune diseases. Furthermore, we found that the metabolic reprogramming observed in Pik3ip1-deficient T cells was mediated by the consistent up-regulation of Hif1α. Emerging evidence has shown that Hif1α has been involved in the pathogenesis of many T cell–associated autoimmune diseases, including SLE, RA, MS, psoriasis, type 1 diabetes mellitus (T1DM), and inflammatory bowel disease (*49*). Thus, our results have shown huge promise in modulating Pik3ip1/Hif1α/glycolysis axis as a potential therapeutic approach for autoimmune conditions. Although other negative immune regulators, such as PD-1, CTLA-4, and LAG-3, also inhibit T cell glycolysis and play an important role in modulating T cell metabolic fitness (*50*–*52*), Pik3ip1 is shown to be the first identified negative immune regulator that mediates metabolic regulation in the autoimmune setting.

We also investigated the possible mechanisms that regulated the expression of Pik3ip1 during autoimmunity. Our studies revealed that neither IL-2, a classical proinflammatory cytokine, nor IFN-α, which shows significant impact on PD-1 expression (*53*), was able to affect the expression of Pik3ip1 in vitro. Unexpectedly, when stimulated with IL-21, T cells showed a rapid decrease in the expression of Pik3ip1 protein, which was similar to T cells stimulated with anti-CD3/CD28 antibodies. Mechanistically, this IL-21–mediated Pik3ip1 regulation was relied on p38 MAPK activation. p38 MAPK has been found to contribute to the elevation of ADAM17 expression and activating ADAM17 by phosphorylating its intercellular domain at tyrosine-735 (*54*). The ability of ADAM17 to induce the down-regulation of Pik3ip1 was reported previously in D10.G4.1 T cells (*16*). The clarification of mechanisms underlying Pik3ip1 expression offers potential targets for manipulating Pik3ip1 under autoimmune conditions. Furthermore, IL-21, mainly produced by T_H17 and T follicular helper cells, plays an essential role in inflammatory and autoimmune diseases, as it contributes to increasing the stochastic opportunities for self-antigen recognition by T cells and promoting T_H17 differentiation (*26*, *55*, *56*). Here, we observed an apparent negative correlation between the percentage of Pik3ip1$^+$ T cells and the percentage of IL-17–producing CD4$^+$ T cells in autoimmune patients and more T_H17 infiltration in *Pik3ip1* cKO mice during EAE. These results might indicate a positive feedback loop, in which the loss of Pik3ip1 enhances IL-21 secretion and, in turn, further dampens the Pik3ip1 level. Thus, targeting Pik3ip1, the critical regulator of this process, might help to inhibit the amplification of uncontrolled immune response and the sustained autoimmune inflammation.

In conclusion, our findings provide previously unidentified insights into the mechanisms underlying the critical metabolic switch of peripheral T cells in the scenario of autoimmunity. We have demonstrated that Pik3ip1, a newly reported negative immune regulators primarily expressed in T cells, contributes to suppressing the development of multiple autoimmune diseases via inhibiting Hif1α-mediated metabolic programming, thereby preventing T cells from aberrant activation and acquiring hyperactive phenotype. Our data support a Pik3ip1-centered inflammatory loop, where Pik3ip1 is down-regulated by IL-21/p38 MAPK/ADAM17 pathway and the down-regulation of Pik3ip1 further exacerbates the autoinflammatory condition. Collectively, such information paves the way for the use of Pik3ip1/Hif1α/glycolysis axis as a potential therapeutic approach in the treatment of autoimmune diseases and for future studies aimed at clarifying critical factors that block the inflammatory feedback loop, which is implicated in many autoimmune diseases.

MATERIALS AND METHODS

Clinical samples

Patients with SLE (n = 57), RA (n = 28), and MS (n = 28) were collected at the Third Affiliated Hospital of Sun Yat-sen University in our study. Patients with hepatitis B virus, hepatitis C virus, HIV, or other bacterial infections were excluded in this study. Demographic and clinical characteristics of the patients are shown in table S1. Meanwhile, age- and sex-matched HDs (n = 10) were enrolled. Whole blood samples were obtained before the initiation of treatment and after 4 weeks of treatment (except for six matched posttreatment patients with MS to assess the effect of treatment on the expression of Pik3ip1). The study was approved by the ethics committee of Stomatological Hospital and the Third Affiliated Hospital of Sun Yat-sen University. Written informed consent was obtained from all of the participants, according to the Declaration of Helsinki.

Mice

C57BL/6 mice were purchased from the experimental animal center of Sun Yat-sen University (Guangzhou, Guangdong, P.R. China). *Pik3ip1*$^{flox/\ flox}$ mice (control) were created in C57BL/6 mice by inserting LoxP on both sides of the exon of *Pik3ip1*. CD4^{Cre} mice were a gift from J. Zhou (Sun Yat-sen University). T cell–specific *Pik3ip1*-deficient mice (cKO) were achieved by crossing *Pik3ip1*$^{flox/\ flox}$ mice to CD4^{Cre} mice. Deletion of Pik3ip1 on T cells was further confirmed by PCR and Western blotting. All mice were maintained in specific pathogen–free facilities of the Sun Yat-sen University. All animal studies were approved and performed according to the Institutional Animal Care and Use Committee guidelines.

EAE model establishment

To induce EAE, 6- to 8-week-old female cKO and control mice were immunized with MOG35-55 (2 mg/ml; Sigma-Aldrich) and *Mycobacterium tuberculosis* (8 mg/ml; BD Biosciences) and dissolved in complete Freund's adjuvant (Sigma-Aldrich) subcutaneously. Immediately after the immunization and again 2 days later, 250 ng of pertussis toxin (MedChemExpress) was administered intraperitoneally. Clinical signs after EAE immunization are according to the following criteria: 0, no signs of disease; 0.5, loss of tail tip tonicity; 1, loss of whole tail tonicity; 2, mild paralysis of hind limbs; 2.5, one hind limb paralysis completely; 3, complete paralysis of both hind limbs; 3.5, hind limbs paralysis and mild paralysis of forelimbs; 4, complete paralysis; and 5, death. Mice were injected with sodium pentobarbital (100 mg/kg body weight) and euthanized through cardiac perfusion with 30 ml of phosphate-buffered saline (PBS) at day 28. After perfusion, the spinal cord, brain, and spleen were dissected and fixed in 4% paraformaldehyde for paraffin sectioning or mechanically disrupted to obtained single-cell suspensions. Mononuclear cells were isolated from these cell suspensions using Percoll.

Flow cytometry and cell sorting

Single-cell preparations were incubated in PBS with 2% serum and Fc block (10 μg/ml; Bio X Cell) for 10 min on ice before staining with antibodies. Cells were stained for dead cells with Ghost Dye Red 780

(Tonbo Biosciences) for 15 min at room temperate in PBS. Surface marker was stained for 30 min at 4°C in PBS with 2% fetal bovine serum. For the intracellular cytokine staining, cells were stimulated in vitro with cell stimulation cocktail for 5 hours at 37°C with 5% CO_2 before staining. Next, cells were fixed and permeabilized with fixation and permeabilization buffer set (Tonbo Biosciences), after which they were stained with intracellular cytokine antibodies according to the manufacturer's instructions. For intranuclear staining, the nuclear membranes were permeabilized with the Foxp3/Transcription Factor Staining Buffer Kit (eBioscience) before transcription factor staining. All analyses were performed on a LSRFortessa instrument (BD Biosciences). Data were processed using FlowJo software. Cell sorting was performed on a FACSAria (BD Biosciences). The antibodies and commercial assays are displayed in table S2.

Gene signature analysis on single-cell and bulk RNA-seq data from the Gene Expression Omnibus database

The single-cell sequencing data used were from GSE157278 (www.ncbi.nlm.nih.gov/geo/query/acc.cgi?acc=GSE157278). The supplementary files from the repository were used as input and processed using the Seurat package. The mitochondrial genes and cells with fewer than 1000 positive read counts were removed. Module scores for each of the gene signatures were used to color the cells on the uniform manifold approximation and projection created from the Seurat processing. The bulk RNA-seq data of SLE, RA, MS, and SS (fig. S1B) were from GSE61635, GSE93272, GSE146383, and GSE66795, respectively. The bulk RNA-seq data of SLE, RA, and MS (Fig. 1B) were from GSE65391, GSE45291, and GSE146383, respectively. The bulk RNA-seq data of SLE, RA, and MS (fig. S1J) were from GSE61635, GSE45291, and GSE24427, respectively. The bulk RNA-seq data of SLE, RA, SS, and SJIA (fig. S4A) were from GSE61635, GSE45291, GSE66795, and GSE80060, respectively.

mRNA-RNA sequencing and analysis

Pik3ip1$^+$ or Pik3ip1$^-$ T cells in the spleen of three mice were selected by flow cytometry and then sent to Guangzhou Magigen Biotechnology Co. Ltd. for total RNA-seq. PC analysis and GSEA of Pik3ip1$^+$ or Pik3ip1$^-$ T cells transcriptome were performed with OmicStudio (www.omicstudio.cn/tool). Heatmap of differentiation in gene expression of selected genes was completed with pheatmap R package. Venn diagram was completed after removing fragments per kilobase of exon per million mapped fragments of <1 genes of each group.

Metabolic assays

Mitochondrial stress test and glycolytic stress test were performed in an XFe96 extracellular flux analyzer. Purity CD4$^+$ and CD8$^+$ T cells of control and cKO mice were used for mitochondrial stress test in Seahorse XF Base Medium (Agilent) added with 10 mM glucose, 2 mM L-glutamine, and 1 mM sodium pyruvate with XF Cell Mito Stress Kit (Agilent). Glycolytic stress test was performed on stimulated CD4$^+$ and CD8$^+$ T cells in Seahorse XF Base Medium added with 2 mM L-glutamine and 1 mM sodium pyruvate with XF Cell Glycolytic Stress Kit (Agilent). All XFe96 FluxPaks (Agilent) were coated with poly-L-lysine (ScienCell) before cell seeding. These plates were centrifuged at 300*g* for 1 min without brakes. OCR of control and cKO CD4$^+$ and CD8$^+$ T cells was measured during sequential injections of oligomycin, carbonyl cyanide *p*-trifluoromethoxyphenylhydrazone (FCCP), and antimycin A/rotenone. OCR was obtained at baseline, maximal OCR was measured after FCCP injection, spare respiratory capacity was calculated as the difference between the maximal and basal OCRs, and ATP production was calculated as the difference between OCRs before and after oligomycin injection. ECAR of control and cKO CD4$^+$ and CD8$^+$ T cells was measured during sequential injections of glucose, oligomycin, and 2-DG. Glycolytic capacity was measured after oligomycin injection, and glycolytic reserve was calculated as the difference between maximal and basal ECARs. The stimulated T cells were also detected by lactic acid with lactic acid content detection kit (SolarBio). Acetyl-CoA detection was performed with liquid chromatography (Agilent).

Function and structure of mitochondria investigation

Purified CD4$^+$ and CD8$^+$ T cells from cKO or control were stained with TMRM (US Everbright Inc.) for confocal analysis and flow cytometry detection to determine mitochondrial membrane potential ($\Delta\Psi$m). Mitochondrial crystal morphology of purified T cells from cKO and control mice was observed with transmission electron microscopy (JEOL). Average number and length of mitochondrial cristae were analyzed by two independent observers blinded to the test.

RNA isolation and RT-qPCR

Total RNA was collected using the RNeasy Mini Kit (Omega) and quantified with the NanoDrop (Thermo Fisher Scientific). cDNA was synthesized from isolated RNA with PrimeScript RT Master Mix (Takara). RT-qPCR was performed using ABI QuantStudio5 System. All RT-qPCR primer sequences are listed in table S3.

Confocal microscopy

For mitochondrial membrane potential analysis, purified CD4$^+$ or CD8$^+$ T cells from cKO or control mice were stained with TMRM and Hoechst 33342 (Beyotime). For Pik3ip1 and ADAM17 detection, purified CD4$^+$ or CD8$^+$ T cell from cKO or control mice were treated with or without anti-CD3/CD28 (BioLegend), IL-21, or p38 MAPK inhibitors (SB203580, Sigma-Aldrich) for 1 hour before staining with antibodies. The samples were detected by Olympus FV3000 confocal microscopy. All antibodies for confocal microscopy are listed in table S2.

Western blotting

Purity T cells from the spleen of cKO or control mice were extracted. Proteins per well were loaded into polyacrylamide gel electrophoresis and sequentially transferred to polyvinylidene fluoride (PVDF) membranes (Bio-Rad). After that, PVDF membranes were further incubated with antibodies. Protein was detected with chemiluminescent substrate system (LumiGLO). All tests were repeated in triplicate on three different days.

Stimulator and inhibitor

For down-regulating the expression of Pik3ip1, purity T cells were stimulated with IL-2 (20 U/ml; PeproTech), IFN-α (500 U/ml; Sino Biological), anti-CD3/CD28 (3 μg/ml; BioLegend), or IL-21 (300 ng/ml; PeproTech) for 0, 15, 30, 45, and 60 min. For activating T cells in vitro for flow cytometry, purified T cells (200,000 cells per well) were cultured in 96-well flat-bottom plates coated with anti-CD3/CD28 antibody (1.5 μg/ml) for 72 hours before staining with antibodies. For activating T cells in vitro for RT-qPCR, purified T cells were cultured with anti-CD3/CD28 antibody (3 μg/ml) for 4 hours. Hif1a inhibitor (BAY87-2243, GlpBio) was used at a concentration of 1 μM in vitro, while BAY87-2243 were given an intragastric administration of 4 mg/kg per day in vivo. For mTOR inhibiting,

10 nM rapamycin (Sigma-Aldrich) was using to treat T cells for 72 hours. For p38 MAPK inhibiting, 20 μM p38 MAPK inhibitor (SB203580, Sigma-Aldrich) was used in vitro.

Statistical methods

All statistical analyses were performed using Prism software (GraphPad). Unpaired or paired Student's tests (two-group comparisons) and one-way analysis of variance (ANOVA) analysis (multiple-group comparisons) were used in data analysis. For EAE clinical score analysis, repeated-measures ANOVA were performed. All tests were two tailed, and $P < 0.05$ was considered significant and represented as $*P < 0.05$; $**P < 0.01$; $***P < 0.001$; $****P < 0.0001$.

SUPPLEMENTARY MATERIALS

Supplementary material for this article is available at https://science.org/doi/10.1126/sciadv.abo4250

View/request a protocol for this paper from *Bio-protocol*.

REFERENCES AND NOTES

1. A. N. Theofilopoulos, D. H. Kono, R. Baccala, The multiple pathways to autoimmunity. *Nat. Immunol.* **18**, 716–724 (2017).
2. J. A. Bluestone, H. Bour-Jordan, M. Cheng, M. Anderson, T cells in the control of organ-specific autoimmunity. *J. Clin. Invest.* **125**, 2250–2260 (2015).
3. L. Duan, X. Rao, K. R. Sigdel, Regulation of inflammation in autoimmune disease. *J. Immunol. Res.* **2019**, 7403796 (2019).
4. C. D. Moorman, S. J. Sohn, H. Phee, Emerging therapeutics for immune tolerance: Tolerogenic vaccines, T cell therapy, and IL-2 therapy. *Front. Immunol.* **12**, 657768 (2021).
5. M. Romano, G. Fanelli, C. J. Albany, G. Giganti, G. Lombardi, Past, present, and future of regulatory T cell therapy in transplantation and autoimmunity. *Front. Immunol.* **10**, 43 (2019).
6. E. L. Pearce, M. C. Poffenberger, C.-H. Chang, R. G. Jones, Fueling immunity: Insights into metabolism and lymphocyte function. *Science* **342**, 1242454 (2013).
7. G. R. Bantug, L. Galluzzi, G. Kroemer, C. Hess, The spectrum of T cell metabolism in health and disease. *Nat. Rev. Immunol.* **18**, 19–34 (2018).
8. G. Soto-Heredero, M. M. G. de Las Heras, E. Gabandé-Rodríguez, J. Oller, M. Mittelbrunn, Glycolysis–A key player in the inflammatory response. *FEBS J.* **287**, 3350–3369 (2020).
9. M. Peng, N. Yin, S. Chhangawala, K. Xu, C. S. Leslie, M. O. Li, Aerobic glycolysis promotes T helper 1 cell differentiation through an epigenetic mechanism. *Science* **354**, 481–484 (2016).
10. V. Kalia, Y. Yuzefpolskiy, A. Vegaraju, H. Xiao, F. Baumann, S. Jatav, C. Church, M. Prlic, A. Jha, P. Nghiem, S. Riddell, S. Sarkar, Metabolic regulation by PD-1 signaling promotes long-lived quiescent CD8 T cell memory in mice. *Sci. Transl. Med.* **13**, eaba6006 (2021).
11. C. H. Chang, J. Qiu, D. O'Sullivan, M. D. Buck, T. Noguchi, J. D. Curtis, Q. Chen, M. Gindin, M. M. Gubin, G. J. W. van der Windt, E. Tonc, R. D. Schreiber, E. J. Pearce, E. L. Pearce, Metabolic competition in the tumor microenvironment is a driver of cancer progression. *Cell* **162**, 1229–1241 (2015).
12. B. Bengsch, A. L. Johnson, M. Kurachi, P. M. Odorizzi, K. E. Pauken, J. Attanasio, E. Stelekati, L. M. McLane, M. A. Paley, G. M. Delgoffe, E. J. Wherry, Bioenergetic insufficiencies due to metabolic alterations regulated by the inhibitory receptor PD-1 are an early driver of $CD8^+$ T cell exhaustion. *Immunity* **45**, 358–373 (2016).
13. H. A. Blair, E. D. Deeks, Abatacept: A review in rheumatoid arthritis. *Drugs* **77**, 1221–1233 (2017).
14. Z. Zhu, X. He, C. Johnson, J. Stoops, A. E. Eaker, D. S. Stoffer, A. Bell, R. Zarnegar, M. C. DeFrances, PI3K is negatively regulated by PIK3IP1, a novel p110 interacting protein. *Biochem. Biophys. Res. Commun.* **358**, 66–72 (2007).
15. X. He, Z. Zhu, C. Johnson, J. Stoops, A. E. Eaker, W. Bowen, M. C. DeFrances, PIK3IP1, a negative regulator of PI3K, suppresses the development of hepatocellular carcinoma. *Cancer Res.* **68**, 5591–5598 (2008).
16. U. U. Uche, A. R. Piccirillo, S. Kataoka, S. J. Grebinoski, L. M. D'Cruz, L. P. Kane, PIK3IP1/TrIP restricts activation of T cells through inhibition of PI3K/Akt. *J. Exp. Med.* **215**, 3165–3179 (2018).
17. M. C. DeFrances, D. R. Debelius, J. Cheng, L. P. Kane, Inhibition of T-cell activation by PIK3IP1. *Eur. J. Immunol.* **42**, 2754–2759 (2012).
18. Y. Chen, J. Wang, X. Wang, X. Li, J. Song, J. Fang, X. Liu, T. Liu, D. Wang, Q. Li, S. Wen, D. Ma, J. Xia, L. Luo, S. G. Zheng, J. Cui, G. Zeng, L. Chen, B. Cheng, Z. Wang, Pik3ip1 is a negative immune regulator that inhibits antitumor T-cell immunity. *Clin. Cancer Res.* **25**, 6180–6194 (2019).
19. X. Han, M. D. Vesely, W. Yang, M. F. Sanmamed, T. Badri, J. Alawa, F. López-Giráldez, P. Gaule, S. W. Lee, J.-P. Zhang, X. Nie, A. Nassar, A. Boto, D. B. Flies, L. Zheng, T. K. Kim, G. W. Moeckel, J. M. McNiff, L. Chen, PD-1H (VISTA)-mediated suppression of autoimmunity in systemic and cutaneous lupus erythematosus. *Sci. Transl. Med.* **11**, (2019).
20. B. Wan, H. Nie, A. Liu, G. Feng, D. He, R. Xu, Q. Zhang, C. Dong, J. Z. Zhang, Aberrant regulation of synovial T cell activation by soluble costimulatory molecules in rheumatoid arthritis. *J. Immunol.* **177**, 8844–8850 (2006).
21. A. P. Cope, H. Schulze-Koops, M. Aringer, The central role of T cells in rheumatoid arthritis. *Clin. Exp. Rheumatol.* **25**, S4–S11 (2007).
22. V. R. Moulton, G. C. Tsokos, T cell signaling abnormalities contribute to aberrant immune cell function and autoimmunity. *J. Clin. Investig.* **125**, 2220–2227 (2015).
23. I. Raphael, S. Nalawade, T. N. Eagar, T. G. Forsthuber, T cell subsets and their signature cytokines in autoimmune and inflammatory diseases. *Cytokine* **74**, 5–17 (2015).
24. X. Hong, S. Meng, D. Tang, T. Wang, L. Ding, H. Yu, H. Li, D. Liu, Y. Dai, M. Yang, Single-cell RNA sequencing reveals the expansion of cytotoxic $CD4^+$ T lymphocytes and a landscape of immune cells in primary Sjögren's syndrome. *Front. Immunol.* **11**, 594658 (2021).
25. A. R. Rodrigues, R. Soares, Inflammation in Sjögren's syndrome: Cause or consequence? *Autoimmunity* **50**, 141–150 (2017).
26. D. Long, Y. Chen, H. Wu, M. Zhao, Q. Lu, Clinical significance and immunobiology of IL-21 in autoimmunity. *J. Autoimmun.* **99**, 1–14 (2019).
27. M. Rizzi, R. Lorenzetti, K. Fischer, J. Staniek, I. Janowska, A. Troilo, V. Strohmeier, M. Erlacher, M. Kunze, B. Bannert, D. Kyburz, R. E. Voll, N. Venhoff, J. Thiel, Impact of tofacitinib treatment on human B-cells in vitro and in vivo. *J. Autoimmun.* **77**, 55–66 (2017).
28. F. Jadidi-Niaragh, A. Mirshafiey, Th17 cell, the new player of neuroinflammatory process in multiple sclerosis. *Scand. J. Immunol.* **74**, 1–13 (2011).
29. N. M. Chapman, H. Chi, Hallmarks of T-cell exit from quiescence. *Cancer Immunol. Res.* **6**, 502–508 (2018).
30. S. E. Corcoran, L. A. J. O'Neill, HIF1α and metabolic reprogramming in inflammation. *J. Clin. Invest.* **126**, 3699–3707 (2016).
31. R. Wang, C. P. Dillon, L. Z. Shi, S. Milasta, R. Carter, D. Finkelstein, L. L. McCormick, P. Fitzgerald, H. Chi, J. Munger, D. R. Green, The transcription factor Myc controls metabolic reprogramming upon T lymphocyte activation. *Immunity* **35**, 871–882 (2011).
32. K. Man, M. Miasari, W. Shi, A. Xin, D. C. Henstridge, S. Preston, M. Pellegrini, G. T. Belz, G. K. Smyth, M. A. Febbraio, S. L. Nutt, A. Kallies, The transcription factor IRF4 is essential for TCR affinity-mediated metabolic programming and clonal expansion of T cells. *Nat. Immunol.* **14**, 1155–1165 (2013).
33. K. Xie, Y. Q. Chen, Y. S. Chai, S. H. Lin, C. J. Wang, F. Xu, HMGB1 suppress the expression of IL-35 by regulating naïve $CD4^+$ T cell differentiation and aggravating caspase-11-dependent pyroptosis in acute lung injury. *Int. Immunopharmacol.* **91**, 107295 (2021).
34. S. C. Land, A. R. Tee, Hypoxia-inducible factor 1alpha is regulated by the mammalian target of rapamycin (mTOR) via an mTOR signaling motif. *J. Biol. Chem.* **282**, 20534–20543 (2007).
35. P. Ellinghaus, I. Heisler, K. Unterschemmann, M. Haerter, H. Beck, S. Greschat, A. Ehrmann, H. Summer, I. Flamme, F. Oehme, K. Thierauch, M. Michels, H. Hess-Stumpp, K. Ziegelbauer, BAY 87-2243, a highly potent and selective inhibitor of hypoxia-induced gene activation has antitumor activities by inhibition of mitochondrial complex I. *Cancer Med.* **2**, 611–624 (2013).
36. A. C. Codo, G. G. Davanzo, L. de Brito Monteiro, G. F. de Souza, S. P. Muraro, J. V. Virgilio-da-Silva, J. S. Prodonoff, V. C. Carregari, C. A. O. de Biagi Junior, F. Crunfli, J. L. J. Restrepo, P. H. Vendramini, G. Reis-de-Oliveira, K. B. Dos Santos, D. A. Toledo-Teixeira, P. L. Parise, M. C. Martini, R. E. Marques, H. R. Carmo, A. Borin, L. D. Coimbra, V. O. Boldrini, N. S. Brunetti, A. S. Vieira, E. Mansour, R. G. Ulaf, A. F. Bernardes, T. A. Nunes, L. C. Ribeiro, A. C. Palma, M. V. Agrela, M. L. Moretti, A. C. Sposito, F. B. Pereira, L. A. Velloso, M. A. R. Vinolo, A. Damasio, J. L. Proença-Módena, R. F. Carvalho, M. A. Mori, D. Martins-de-Souza, H. I. Nakaya, A. S. Farias, P. M. Moraes-Vieira, Elevated glucose levels favor SARS-CoV-2 infection and monocyte response through a HIF-1α/glycolysis-dependent axis. *Cell Metab.* **32**, 437–446.e5 (2020).
37. J. L. Grant, E. E. B. Ghosn, R. C. Axtell, K. Herges, H. F. Kuipers, N. S. Woodling, K. Andreasson, L. A. Herzenberg, L. A. Herzenberg, L. Steinman, Reversal of paralysis and reduced inflammation from peripheral administration of β-amyloid in TH1 and TH17 versions of experimental autoimmune encephalomyelitis. *Sci. Transl. Med.* **4**, 145ra105 (2012).
38. A. Geraud, P. Gougis, A. Vozy, C. Anquetil, Y. Allenbach, E. Romano, E. Funck-Brentano, J. J. Moslehi, D. B. Johnson, J. E. Salem, Clinical pharmacology and interplay of immune checkpoint agents: A yin-yang balance. *Annu. Rev. Pharmacol. Toxicol.* **61**, 85–112 (2021).
39. N. Joller, J. P. Hafler, B. Brynedal, N. Kassam, S. Spoerl, S. D. Levin, A. H. Sharpe, V. K. Kuchroo, Cutting edge: TIGIT has T cell-intrinsic inhibitory functions. *J. Immunol.* **186**, 1338–1342 (2011).
40. H. Nishimura, M. Nose, H. Hiai, N. Minato, T. Honjo, Development of lupus-like autoimmune diseases by disruption of the PD-1 gene encoding an ITIM motif-carrying immunoreceptor. *Immunity* **11**, 141–151 (1999).

41. K. Klocke, S. Sakaguchi, R. Holmdahl, K. Wing, Induction of autoimmune disease by deletion of CTLA-4 in mice in adulthood. *Proc. Natl. Acad. Sci. U.S.A.* **113**, E2383–E2392 (2016).
42. M. Bettini, A. L. Szymczak-Workman, K. Forbes, A. H. Castellaw, M. Selby, X. Pan, C. G. Drake, A. J. Korman, D. A. A. Vignali, Cutting edge: Accelerated autoimmune diabetes in the absence of LAG-3. *J. Immunol.* **187**, 3493–3498 (2011).
43. M. D. Buck, D. O'Sullivan, E. L. Pearce, T cell metabolism drives immunity. *J. Exp. Med.* **212**, 1345–1360 (2015).
44. Y. Yin, S.-C. Choi, Z. Xu, D. J. Perry, H. Seay, B. P. Croker, E. S. Sobel, T. M. Brusko, L. Morel, Normalization of $CD4^+$ T cell metabolism reverses lupus. *Sci. Transl. Med.* **7**, 274ra218 (2015).
45. Z. Zhang, Z. Zi, E. E. Lee, J. Zhao, D. C. Contreras, A. P. South, E. D. Abel, B. F. Chong, T. Vandergriff, G. A. Hosler, P. E. Scherer, M. Mettlen, J. C. Rathmell, R. J. DeBerardinis, R. C. Wang, Differential glucose requirement in skin homeostasis and injury identifies a therapeutic target for psoriasis. *Nat. Med.* **24**, 617–627 (2018).
46. W. Li, G. Qu, S.-C. Choi, C. Cornaby, A. Titov, N. Kanda, X. Teng, H. Wang, L. Morel, Targeting T cell activation and lupus autoimmune phenotypes by inhibiting glucose transporters. *Front. Immunol.* **10**, 833 (2019).
47. T. Okano, J. Saegusa, K. Nishimura, S. Takahashi, S. Sendo, Y. Ueda, A. Morinobu, 3-Bromopyruvate ameliorate autoimmune arthritis by modulating Th17/Treg cell differentiation and suppressing dendritic cell activation. *Sci. Rep.* **7**, 42412 (2017).
48. S. Telang, B. F. Clem, A. C. Klarer, A. L. Clem, J. O. Trent, R. Bucala, J. Chesney, Small molecule inhibition of 6-phosphofructo-2-kinase suppresses t cell activation. *J. Transl. Med.* **10**, 95 (2012).
49. S. Y. Guan, R.-X. Leng, J.-H. Tao, X.-P. Li, D.-Q. Ye, N. Olsen, S. G. Zheng, H.-F. Pan, Hypoxia-inducible factor-1α: A promising therapeutic target for autoimmune diseases. *Expert Opin. Ther. Targets* **21**, 715–723 (2017).
50. D. M. Previte, C. P. Martins, E. C. O'Connor, M. L. Marre, G. M. Coudriet, N. W. Beck, A. V. Menk, R. H. Wright, H. M. Tse, G. M. Delgoffe, J. D. Piganelli, Lymphocyte activation gene-3 maintains mitochondrial and metabolic quiescence in naive $CD4^+$ T cells. *Cell Rep.* **27**, 129–141.e4 (2019).
51. N. Patsoukis, K. Bardhan, P. Chatterjee, D. Sari, B. Liu, L. N. Bell, E. D. Karoly, G. J. Freeman, V. Petkova, P. Seth, L. Li, V. A. Boussiotis, PD-1 alters T-cell metabolic reprogramming by inhibiting glycolysis and promoting lipolysis and fatty acid oxidation. *Nat. Commun.* **6**, 6692 (2015).
52. R. Zappasodi, I. Serganova, I. J. Cohen, M. Maeda, M. Shindo, Y. Senbabaoglu, M. J. Watson, A. Leftin, R. Maniyar, S. Verma, M. Lubin, M. Ko, M. M. Mane, H. Zhong, C. Liu, A. Ghosh, M. Abu-Akeel, E. Ackerstaff, J. A. Koutcher, P.-C. Ho, G. M. Delgoffe, R. Blasberg, J. D. Wolchok, T. Merghoub, CTA-4 blockade drives loss of T_{reg} stability in glycolysis-low tumours. *Nature* **591**, 652–658 (2021).
53. S. Terawaki, S. Chikuma, S. Shibayama, T. Hayashi, T. Yoshida, T. Okazaki, T. Honjo, IFN-α directly promotes programmed cell death-1 transcription and limits the duration of T cell-mediated immunity. *J. Immunol.* **186**, 2772–2779 (2011).
54. E. Thorp, T. Vaisar, M. Subramanian, L. Mautner, C. Blobel, I. Tabas, Shedding of the Mer tyrosine kinase receptor is mediated by ADAM17 protein through a pathway involving reactive oxygen species, protein kinase Cδ, and p38 mitogen-activated protein kinase (MAPK). *J. Biol. Chem.* **286**, 33335–33344 (2011).
55. J. L. Jones, C.-L. Phuah, A. L. Cox, S. A. Thompson, M. Ban, J. Shawcross, A. Walton, S. J. Sawcer, A. Compston, A. J. Coles, IL-21 drives secondary autoimmunity in patients with multiple sclerosis, following therapeutic lymphocyte depletion with alemtuzumab (Campath-1H). *J. Clin. Invest.* **119**, 2052–2061 (2009).
56. G. Geri, B. Terrier, M. Rosenzwajg, B. Wechsler, M. Touzot, D. Seilhean, T.-A. Tran, B. Bodaghi, L. Musset, V. Soumelis, D. Klatzmann, P. Cacoub, D. Saadoun, Critical role of IL-21 in modulating TH17 and regulatory T cells in Behçet disease. *J. Allergy Clin. Immunol.* **128**, 655–664 (2011).

Acknowledgments: We thank J. Zhou (Sun Yat-sen University) for the gift of $CD4^{Cre}$ mice. **Funding:** This study was funded by National Natural Science Foundation of PR China (nos. 81972532, 81991500, 82101017, and 81802403). **Author contributions:** Conceptualization: Z.W., J.F., and W.X. Data curation: W.X. and Z.S. Formal analysis: W.X. and Z.S. Funding acquisition: Z.W., J.F., and Y.L. Investigation: W.X., Z.S., Z.Z., J.W., Y.Z., and J.G. Methodology: W.X., Z.S., S.W., H.L., L.Y., and Y.Z. Project administration: Z.W. Resources: Z.W., J.F., H.Z., and Y.L. Software: J.G. and H.L. Supervision: Z.W., Q.C., and D.-M.K. Validation: S.W. Visualization: J.G. Writing: Z.W., J.G., P.H., and W.X. **Competing interests:** The authors declare that they have no competing interests. **Data and materials availability:** All data needed to evaluate the conclusions in the paper are present in the paper and/or the Supplementary Materials.

Submitted 3 February 2022
Accepted 17 August 2022
Published 30 September 2022
10.1126/sciadv.abo4250